NIST

United States Department of Commerce
Technology Administration
National Institute of Standards and Technology

NISTIR 3981

SIMULATION OF THE MERGED SPECTRUM TECHNIQUE FOR ALIGNING PLANAR PHASED-ARRAY ANTENNAS, PART I

Ronald C. Wittmann
Allen C. Newell
Carl F. Stubenrauch
Katherine MacReynolds
Michael H. Francis

SIMULATION OF THE MERGED SPECTRUM TECHNIQUE FOR ALIGNING PLANAR PHASED-ARRAY ANTENNAS, PART I

Ronald C. Wittmann
Allen C. Newell
Carl F. Stubenrauch
Katherine MacReynolds
Michael H. Francis

Electromagnetic Fields Division
Electronics and Electrical Engineering Laboratory
National Institute of Standards and Technology
Boulder, Colorado 80303-3328

October 1992

CONTENTS

LIST OF FIGURES

Figure   Page

iv

Figure   Page

SIMULATION OF THE MERGED-SPECTRUM TECHNIQUE
FOR ALIGNING PLANAR PHASED-ARRAY ANTENNAS,
PART I

Ronald C. Wittmann

Allen C. Newell

Carl F. Stubenrauch

Katherine MacReynolds

Michael H. Francis

Electromagnetic Fields Division

National Institute of Standards and Technology

Boulder, CO 80303-3328

This report describes the initial phase of a NIST study of the merged-spectrum technique for determining the element excitations from planar scanning near-field measurements of phased-array antennas. Excitation data are used in adjusting phase shifters to meet design specifications. Measurement uncertainties, steering errors, and various analytic approximations will all introduce errors into the alignment. The study is ultimately directed to quantify the effect of these errors, to more fully understand the merged-spectrum technique, and to recommend possible improvements. The present report covers theory developed to support evaluation of the merged-spectrum technique and gives simulation examples illustrating calculation of near fields from array factor and element patterns.

Key words: antenna measurements; antenna array alignment; merged spectrum; near-field measurements; phased-array antennas; planar scanning.

1.0 INTRODUCTION

This report describes the initial phase of a NIST study of a method for determining the element excitations (amplitude and phase) from planar near-field measurements of phased-array antennas. The method is called the merged-spectrum technique because the (broadside-beam) array factor is obtained from several spectra, each measured with the array electrically steered to a different direction [1]. (There may not be enough information in any one spectrum to determine the array factor directly.)

Excitation data are used in adjusting phase shifters, which initially may be set randomly, to meet design specifications. Measurement uncertainties, steering errors, and various analytic approximations will all introduce errors into the alignment. The study is ultimately directed to quantify the effect of these errors, to more fully understand the merged-spectrum technique, and to recommend possible improvements. The present report covers computer code and theory developed to support evaluation of the merged-spectrum technique.

A first step, contained in sections 2 through 4, is a careful description of measurement and theory needed for the merged-spectrum technique. Section 2 is a brief summary of the principles, relations, and notation of the planar near-field scanning measurement technique. In section 3 phased-array antennas are introduced and the concepts of element excitations, average element pattern, and array factor are discussed. The relations between the lattice of array elements and the corresponding reciprocal lattice in k space are developed since these are critical concepts in the merged-spectrum technique. Section 4 sketches the merged-spectrum theory. In section 5 we give some simulation results, illustrating calculation of array factors for steered and unsteered beams, as well as simulated near-field measurements for typical element and probe patterns. Additionally, examples of the effect of certain measurement errors are shown.

2.0 BASIC NEAR-FIELD MEASUREMENT THEORY

The theory of planar near-field scanning is briefly summarized in this section. A thorough account may be found in Kerns [2].

2.1 The Spectral Representation of Radiated Fields

The theory of planar near-field scanning is based on the fact that radiated fields can be written as a superposition of plane waves

$$\mathbf{E}(\mathbf{r}) = \frac{1}{2\pi} \int \mathbf{t}(\hat{\mathbf{k}}) \exp(i\mathbf{k} \cdot \mathbf{r}) \frac{d\mathbf{K}}{\gamma k} , \qquad z > 0, \tag{1}$$

where an $\exp(-i\omega t)$ time dependence is suppressed. Here

$$\mathbf{k} = \mathbf{K} + \gamma \hat{\mathbf{z}} , \qquad \mathbf{K} = k_x \hat{\mathbf{x}} + k_y \hat{\mathbf{y}} , \qquad K = |\mathbf{K}|$$

2

$$\gamma = k_z = \begin{cases} \sqrt{k^2 - K^2}, & k \geq K \\ i\sqrt{K^2 - k^2}, & k < K \end{cases}$$

$$\int d\mathbf{K} \equiv \int_{-\infty}^{\infty} dk_x \int_{-\infty}^{\infty} dk_y .$$

The _far-field pattern_ $t(\hat{\mathbf{r}})$ is defined so that

$$E(\mathbf{r}) \underset{r \longrightarrow \infty}{\sim} t(\hat{\mathbf{r}}) \frac{\exp(ikr)}{ikr} . \tag{2}$$

The quantity $t(\hat{\mathbf{k}})/\gamma k$ is called the _spectrum_ of $E(\mathbf{r})$.

2.2 Kerns's Transmission Equation

The output of a probe can be related to the incident field through the transmission equation

$$W(\mathbf{r}) = \int \mathbf{r}(\hat{\mathbf{k}}) \cdot \mathbf{t}(\hat{\mathbf{k}}) \exp(i\mathbf{k} \cdot \mathbf{r}) \frac{d\mathbf{K}}{\gamma k}$$

$$= \int D(\hat{\mathbf{k}}) \exp(i\gamma z) \exp(i\mathbf{K} \cdot \mathbf{r}) d\mathbf{K} , \qquad z > 0 \tag{3}$$

$$D(\hat{\mathbf{k}}) \equiv \mathbf{r}(\hat{\mathbf{k}}) \cdot \mathbf{t}(\hat{\mathbf{k}})/\gamma k .$$

$D(\hat{\mathbf{k}})$ is the _coupling product_. The _receiving pattern_ $\mathbf{r}(\mathbf{k})$ is defined so that the response of the probe to the incident plane wave

$$\frac{1}{2\pi} \mathbf{E}_0 \exp(i\mathbf{k} \cdot \mathbf{r})$$

is

$$\mathbf{r}(\hat{\mathbf{k}}) \cdot \mathbf{E}_0 \exp(i\mathbf{k} \cdot \mathbf{r}_p) ,$$

where $\mathbf{r}_p$ is the position of the probe. The definition of the receiving pattern depends on the choice of probe calibration; however, the details of this normalization are unimportant for the present application.

Basically, the transmission equation states that the probe output is the sum of the probe responses to the plane-wave components of the incident field eq (1).

2.3 Inverting the Transmission Equation

Fourier transformation of eq (3) gives

$$D(\hat{\mathbf{k}}) = \frac{1}{4\pi^2} \int W(\mathbf{r}) \, \exp(-i\mathbf{k} \cdot \mathbf{r}) \, d\mathbf{R} \, , \qquad z > 0 \, , \tag{4a}$$

or

$$D(\hat{\mathbf{k}}) \, \exp(i\gamma z_0) = \frac{1}{4\pi^2} \int W(\mathbf{r}) \, \exp(-i\mathbf{K} \cdot \mathbf{R}) \, d\mathbf{R} \, , \qquad z > 0 \tag{4b}$$

$$\mathbf{r} = \mathbf{R} + z_0 \hat{\mathbf{z}} \, , \qquad \mathbf{R} = x\hat{\mathbf{x}} + y\hat{\mathbf{y}}$$

$$\int d\mathbf{R} \equiv \int_{-\infty}^{\infty} dx \int_{-\infty}^{\infty} dy \, .$$

Thus, in principle, the coupling product may be determined if the probe response is known on a plane $z = z_0 > 0$.

2.4 Sampling the Near Field

The application of eq (4) is greatly simplified by the fact that $D(\hat{\mathbf{k}})$ is strongly spatially bandlimited because the plane-wave components become evanescent when $K > k$. Thus, according to the "sampling theorem," the coupling product may be reconstructed "exactly" from discrete probe measurements as long as the sample interval is less than half a wavelength:

$$\Delta x, \ \Delta y \le \lambda/2 \, . \tag{5}$$

In an actual measurement, of course, the scan area must be finite. A rule of thumb is that every line drawn from the aperture in a direction in which the far field is to be determined must pass through the measurement region. (Like all rules of thumb, this is subject to experimental verification.)

With the assumption of discrete sampling and truncation of the integration range, eq (4) may be reduced to a DFT (Discrete Fourier Transform). By the nature of the DFT (discussed more fully in section 3.5), measurements made at the points

$$\mathbf{r}_{nm} = n\Delta x \; \hat{\mathbf{x}} + m\Delta y \; \hat{\mathbf{y}} + z_0 \; \hat{\mathbf{z}}$$

result in the determination of $D(\hat{\mathbf{k}})$ for

$$\mathbf{K}_{nm} = \frac{n}{N_x} \frac{2\pi}{\Delta x} \; \hat{\mathbf{x}} + \frac{m}{N_y} \frac{2\pi}{\Delta y} \; \hat{\mathbf{y}} \; , \qquad (6)$$

where N_x and N_y are the numbers of data points in the x and y directions. The K space increments Δk_x and Δk_y are inversely proportional to the x and y dimensions of the measurement plane.

It is often useful to zero-fill the data array by explicitly (rather than implicitly) setting the probe response to 0 outside the actual measurement region. This does not add any information, but it does result in evaluation of the coupling product on a finer grid [since N_x and/or N_y have been increased in eq (6)]. Also, the FFT (Fast Fourier Transform) algorithm used to perform the DFT is most efficient if N_x and N_y can be factored into small primes. For example, use $N_x = 256$, but not $N_x = 251$.

3.0 BASIC ARRAY THEORY

This section describes the basic elements of antenna array theory needed for an understanding of the merged-spectrum technique. A good general reference is Ma [3].

3.1 The Fields of a Planar Antenna Array

Consider a planar array made up of identical elements. The electric field of the array is a superposition of the element fields:

$$\mathbf{E}(\mathbf{r}) = \sum_i a(\mathbf{R}_i) \; e(\mathbf{r} - \mathbf{R}_i) \; . \qquad (7)$$

The sum runs over the positions of the array elements $\mathbf{R}_i$. We take

$$\mathbf{R}_i = x_i \hat{\mathbf{x}} + y_i \hat{\mathbf{y}} , \tag{8}$$

so that the array lies in the z = 0 plane. The <u>excitation matrix</u> $a(\mathbf{R}_i)$ determines the amplitude and phase of the element excitations. The beam is shaped and steered by controlling $a(\mathbf{R}_i)$. The <u>average element</u> field $e(\mathbf{r})$ is not the free-space field of an element, but includes effects of mutual interactions among elements and supports, etc. (In a finite array it is an approximation to assume that all elements produce the same effective field since the environment varies from location to location.)

An array element is characterized by a far-field pattern $t^e(\hat{\mathbf{k}})$, which we define so that

$$e(\mathbf{r}) \underset{r \longrightarrow \infty}{\sim} t^e(\hat{\mathbf{r}}) \frac{\exp(ikr)}{ikr} . \tag{9}$$

When an element is positioned in the array, its far-field pattern is multiplied by a phase factor depending on the displacement from the coordinate origin (which is the mathematical "location" of the array):

$$e(\mathbf{r} - \mathbf{R}_i) \underset{r \longrightarrow \infty}{\sim} t^e(\hat{\mathbf{r}}) \exp(-ik\hat{\mathbf{r}} \cdot \mathbf{R}_i) \frac{\exp(ikr)}{ikr} . \tag{10}$$

From eqs (7) and (10)

$$\mathbf{E}(\mathbf{r}) \underset{r \longrightarrow \infty}{\sim} t^a(\hat{\mathbf{r}}) \frac{\exp(ikr)}{ikr} , \tag{11}$$

where $t^a(\hat{\mathbf{r}})$ is given by

$$t^a(\hat{\mathbf{r}}) = t^e(\hat{\mathbf{r}}) \sum_i a(\mathbf{R}_i) \exp(-ik\hat{\mathbf{r}} \cdot \mathbf{R}_i)$$

$$\equiv t^e(\hat{\mathbf{r}}) \; A(k\mathbf{R}/r) . \tag{12}$$

The far-field pattern of the array is the product of the average element far-field pattern and the <u>array factor</u> $A(\hat{\mathbf{r}})$.

According to eq (1), the electric field of the array may be written in terms of its far-field pattern:

$$E(r) = \frac{1}{2\pi} \int t^a(\hat{k}) \exp(ik \cdot r) \frac{dK}{\gamma k}$$

$$= \frac{1}{2\pi} \int t^e(\hat{k}) A(K) \exp(ik \cdot r) \frac{dK}{\gamma k} , \qquad z > 0 \qquad (13)$$

$$A(K) = \sum_i a(R_i) \exp(-iK \cdot R_i) . \qquad (14)$$

3.2 The Array Factor for a Broadside Beam

When the beam is broadside, the $a(R_i)$ must have constant phase since this will maximize the far-field pattern in the z direction: If the broadside-beam excitation matrix and the corresponding array factor are denoted by $\alpha(R_i)$ and $A_0(K)$, respectively, then from eq (14)

$$|A_0(0)| = \sum_i |\alpha(R_i)| \geq |A_0(K)| . \qquad (15)$$

The purpose of the merged-spectrum alignment is to determine the actual values of the $\alpha(R_i)$ for an unaligned array so they may be adjusted to the design values. We will call $A_0(K)$ the form factor of the array. As demonstrated in section 3.3, the array factor of a steered beam is simply related to the form factor.

3.3 Steering the Beam

Steering is accomplished by adjusting the phase of the excitation matrix. When the excitation matrix is

$$a(R_i) = \alpha(R_i) \exp(iK_0 \cdot R_i) , \qquad (16)$$

then the array factor

$$A(K) = A_0(K - K_0) = \sum_i \alpha(R_i) \exp[-i(K - K_0) \cdot R_i] \qquad (17)$$

will produce a beam in the $\hat{k}_0$ direction. With the convention eq (16), the phase of a reference element at the origin will be independent of K_0.

7

The electric field of the steered array is

$$E(r) = \frac{1}{2\pi} \int t^e(\hat{k}) \, A_0(K - K_0) \, \exp(ik \cdot r) \, \frac{dK}{\gamma k} \,, \qquad z > 0 \,. \qquad (18)$$

Since the plane-wave components of eq (18) become evanescent when $K > k$, $A_0(L)$ plays an active role in determining the far field of the array only when L lies within a circle of radius $k = \omega/c$ centered on $L = -K_0$. Thus, the <u>visible</u> portion of the form factor depends on the steering angle.

The steering vector K_0 can be related to the usual polar angles θ and ϕ:

$$K_{0x} = k \sin\theta \, \cos\phi \,, \qquad K_{0y} = k \sin\theta \, \sin\phi$$

$$\sin\theta = K_0/k \,, \qquad \tan\phi = K_{0y}/K_{0x} \,.$$

3.4 The Array Factor for a Regular Lattice

Every point in a planar lattice can be represented in the form

$$R_{nm} = na + mb \qquad (19)$$

($a \times b \neq 0$). The <u>fundamental lattice vectors</u> a and b are said to be <u>primitive</u> if R_{nm} is a lattice point for all integers n and m.

In this report we will assume that the array elements lie on a <u>centered rectangular lattice</u>, illustrated in figure 1, where the fundamental lattice vectors are given by

$$a = \lambda(\frac{1}{2} \hat{x} - \frac{3}{10} \hat{y}) \,, \qquad b = \frac{3}{5}\lambda \, \hat{y} \,. \qquad (20)$$

a and b are clearly primitive. [The choice of a and b is not unique; for example, we could use $a = \lambda(\frac{1}{2} \hat{x} + \frac{3}{10} \hat{y})$.]

The array factor eq (14) may now be written

$$A(K) = \sum_{\nu\mu} a_{\nu\mu} \, \exp(-iK \cdot R_{\nu\mu}) \qquad (21)$$

$$a_{nm} \equiv a(R_{nm}) \,.$$

It is easy to show from eq (21) that the array factor is doubly periodic

8

$$A(K \pm A) = A(K) , \qquad A(K \pm B) = A(K) , \tag{22}$$

where

$$A \equiv 2\pi \frac{b \times \hat{z}}{|a \times b|} = 2k\ \hat{x}, \qquad B \equiv 2\pi \frac{\hat{z} \times a}{|a \times b|} = k(\hat{x} + \frac{5}{3}\ \hat{y}) . \tag{23}$$

[For a rectangular lattice with $a = a\hat{x}$, $b = b\hat{y}$, we have $A = 2\pi/a\ \hat{x}$, $B = 2\pi/b\ \hat{y}$. In general, $|A|$ is proportional to $1/a$ (independent of b) and $|B|$ is proportional to $1/b$ (independent of a).]

A and B are fundamental lattice vectors of the <u>reciprocal lattice</u> shown in figure 2. The form factor $A_0(K)$ assumes its maximum amplitude at each lattice point ($K_{nm} = nA + mB$). Consequently, if more than one reciprocal lattice point is visible, then, in addition to the main beam, there may be other beams (<u>grating lobes</u>) in the far-field pattern. Figure 2 also shows a <u>fundamental period</u> (shaded rectangle) for the array factor. If the array factor is known on a fundamental period then it may be determined everywhere by periodic repetition using eq (22). (While the area is fixed, a fundamental period may assume a number of shapes. A rectangle is convenient for our purposes.)

The preceding discussion assumes that $R = 0$ is a lattice point (that is, there is an element at the origin). If the array is offset so that

$$R_{nm} = \xi + na + mb , \tag{24}$$

then $A(K) \exp(iK \cdot \xi)$ is periodic with periods A and B. Depending on ξ, the array factor itself may have periods which are multiples of A and B, or it may be aperiodic. For instance, when $\xi = b/2$ we have $A(K + B) = -A(K)$ [see eq (29)] corresponding to a period of $2B$.

To gain the convenience of working with rectangular arrays we use the "doubled" lattice shown in figure 3. Because the lattice vectors

$$a' = \frac{1}{2}\lambda\ \hat{x} , \qquad b' = \frac{3}{10}\lambda\ \hat{y} \tag{25}$$

are not primitive with respect to the centered rectangular sublattice, it is necessary to include virtual elements with 0 excitation at the locations

$$R'_{nm} = na' + mb' , \tag{26}$$

9

when n+m is even. (The prime is used to distinguish the doubled lattice from the centered rectangular lattice.)

One effect of using the nonprimitive basis, $\mathbf{a}'$ and $\mathbf{b}'$, is that the fundamental period is doubled in size as shown in figure 4. In addition to the periodicities

$$A(\mathbf{K} \pm \mathbf{A}') = A(\mathbf{K} \pm \mathbf{A}) = A(\mathbf{K}) , \qquad A(\mathbf{K} \pm \mathbf{B}') = A(\mathbf{K}) \tag{27}$$

$$\mathbf{A}' = \mathbf{A} = 2k \; \hat{\mathbf{x}} , \qquad \mathbf{B}' = \frac{10}{3}k \; \hat{\mathbf{y}} , \tag{28}$$

we have

$$A(\mathbf{K} \pm \mathbf{B}) = -A(\mathbf{K}) . \tag{29}$$

The minus sign in eq (29) occurs because the centered rectangular sublattice is offset from the origin. The fundamental period of the doubled lattice can be constructed from the fundamental period of the centered rectangular sublattice using eqs (27) and (29). The mapping is illustrated in figure 4.

3.5 Transforming Between Array Factor and Excitation Matrix

The array factor is given by

$$A(\mathbf{K}) = \sum_{\nu\mu} a'_{\nu\mu} \; \exp(-i\mathbf{K} \cdot \mathbf{R}'_{\nu\mu}) ,$$

where

$$a'_{nm} = a(\mathbf{R}'_{nm}) .$$

To produce the appropriate centered rectangular lattice, a'_{nm} must be 0 when n+m is even ($a'_{00} = 0$).

For convenience in applying the FFT algorithm, we bias the summation indices so they will be positive:

$$A(\mathbf{K}) \; \exp(-i\mathbf{K} \cdot \mathbf{R}'_{NM}) = \sum_{\nu=0}^{P-1} \sum_{\mu=0}^{Q-1} a'_{\nu-N,\mu-M} \; \exp(-i\mathbf{K} \cdot \mathbf{R}'_{\nu\mu}) . \tag{30}$$

Here N and M have been chosen so that $a'_{nm} = 0$ when $n < -N$ or $m < -M$; P and Q have been chosen so that $a'_{n-N,m-M} = 0$ when $n \geq P$ or $m \geq Q$. In effect, a new origin has been chosen so that the reference element coordinates are (N,M).

Let

$$\mathbf{K}_{nm} = \frac{n}{P}\frac{2\pi}{a'}\,\hat{\mathbf{a}}' + \frac{m}{Q}\frac{2\pi}{b'}\,\hat{\mathbf{b}}' = \frac{n}{P}\mathbf{A}' + \frac{m}{Q}\mathbf{B}' \ . \tag{31}$$

Then eq (30) may be rewritten

$$A(\mathbf{K}_{nm})\ \omega_P^{-nN}\ \omega_Q^{-mM} = \sum_{\nu=0}^{P-1}\sum_{\mu=0}^{Q-1} a'_{\nu-N,\mu-M}\ \omega_P^{-\nu n}\ \omega_Q^{-\mu m} \ , \tag{32}$$

where

$$\omega_P \equiv \exp\left(\frac{2\pi i}{P}\right)\ , \qquad \omega_Q \equiv \exp\left(\frac{2\pi i}{Q}\right)\ . \tag{33}$$

If we define

$$A(\mathbf{K}_{nm}) \equiv F_{n+N,m+M}\ \omega_P^{nN}\ \omega_Q^{mM} \tag{34}$$

$$a'_{nm} \equiv f_{n+N,m+M}\ \omega_P^{-(n+N)N}\ \omega_Q^{-(m+M)M} \tag{35}$$

$$-N \leq n \leq P-1-N \ , \quad -M \leq m \leq Q-1-M \ , \tag{36}$$

then eq (32) becomes

$$F_{nm} = \sum_{\nu=0}^{P-1}\sum_{\mu=0}^{Q-1} f_{\nu\mu}\ \omega_P^{-\nu n}\ \omega_Q^{-\mu m} \tag{37}$$

$$f_{nm} = \frac{1}{PQ}\sum_{\nu=0}^{P-1}\sum_{\mu=0}^{Q-1} F_{\nu\mu}\ \omega_P^{\nu n}\ \omega_Q^{\mu m} \ . \tag{38}$$

The sequences F_{nm} and f_{nm} are related by a two-dimensional DFT. The choice of phase factors in eqs (34) and (35) allows use of the natural range for the indices eq (36) without rearrangement of the outputs of the FFT routine.

The transformation between excitation matrix and array factor may be represented schematically as

$$a' \longleftrightarrow \genfrac{}{}{0pt}{}{\text{phase}}{\text{factor}} \longleftrightarrow f \longleftrightarrow \text{FFT} \longleftrightarrow F \longleftrightarrow \genfrac{}{}{0pt}{}{\text{phase}}{\text{factor}} \longleftrightarrow A \ .$$

For the specific case used in the simulation, the excitation matrix (here denoted c_{nm}) is in a row and column format rather than in the cartesian format used in these notes. The relation to the broadside-beam excitation matrix α'_{nm} is

$$\alpha'_{nm} = c_{M+1-m, N+1+n} \ ,$$

where

$$N = 39 \ , \qquad M = 70 \tag{39a}$$

$$P \geq 79 \ , \qquad Q \geq 141 \ . \tag{39b}$$

4.0 THE MERGED-SPECTRUM TECHNIQUE

When the beam is steered to K_0, the visible region of the form factor is a circle of radius k centered on $-K_0$ (see section 3.3). As figure 5 illustrates, when using only a broadside beam, extrapolation is necessary to estimate the form factor. (Coverage does not extend even to radius k since the near-field scan area must be truncated.) From a practical point of view it is better to measure the array factor directly rather than to extrapolate. In the merged-spectrum technique, direct measurement is accomplished by steering the beam to make different regions of the form factor visible. Information from several beams is merged to give the fundamental period. Figure 6 shows an example (discussed below) using four beams.

4.1 Choosing Parameters

Three criteria must be considered:

(1) The density of points in K space must be chosen so that the requirement eq (39b) is satisfied.
(2) The beams should be obtainable without quantization errors in the phase shifters.
(3) The beam directions must be chosen so that data points lie on a common grid in K space.

12

To satisfy criterion (1) we take P = 128 and Q = 256, so the form factor is evaluated at the points

$$K_{nm} = \frac{n}{128} \; A' + \frac{m}{256} \; B' \; . \tag{40}$$

With seven-bit phase shifters, the beam may be steered, without quantization error, to the directions K_{nm} when m is even. Thus, criteria (2) and (3) may be satisfied with the four beam directions

$$K_{\pm32,\pm32} = \pm \frac{1}{4} \; A' \pm \frac{1}{8} \; B' = (\pm \frac{1}{2} \; \hat{x} \pm \frac{5}{12} \; \hat{y})k \tag{41}$$

which are shown in figure 6.

4.2 Determining the Form Factor from Near-Field Data

It is most convenient to collect near-field data so that the DFT will give the array coupling product $D^a(K)$ at appropriate K values without requiring additional interpolation. A comparison of eqs (6) and (31) yields

$$N_x \; \Delta x = 0.5 \; \lambda P$$

$$\tag{42}$$

$$N_y \; \Delta y = 0.3 \; \lambda Q \; .$$

For example, let P = 128 and Q = 256 as in eq (40). The requirements eqs (5) and (42) can be satisfied with the choices $\Delta x = 0.25\lambda$, $\Delta y = 0.3\lambda$, and $N_x = N_y = 256$. The dimensions of the measurement plane are 64λ by 77λ, whereas the array is roughly 42λ in diameter. To determine $A_0(K)$ over a fundamental period, $D^a(K)$ must be known [for each steering angle eq (41)] over the central rectangle of figure 6 ($\theta \leq 40.6°$). According to the truncation criterion of section 2.4, calculated results should be valid in this region if the spacing between scan plane and array is less than about 14λ.

Near-field measurements are transformed in the standard manner (FFT) to obtain $D^a(K_{nm})$. From eqs (3) and (18) we have

$$A_0(K_{nm} - K_0) = D^a(K_{nm})/D^e(K_{nm}) \; , \tag{43}$$

where $D^e(K_{nm})$ is the coupling product between the probe and an "average element." $D^e(K_{nm})$ is determined independently, and it must be known at least

13

for the central rectangular region indicated in figure 6. For each beam
direction eq (43) determines $A_0(\mathbf{K})$ in a disk of radius $K \lesssim k$ about the point
$\mathbf{K} = -\mathbf{K}_0$.

4.3 Combining Beams

One way to combine the spectral information from the beams used in
figure 6 is to simply let each beam determine $A_0(\mathbf{K})$ in the corresponding
quadrant, perhaps averaging along the common boundaries. An alternative
method would be to construct a weighted average in the overlap regions. The
weights would be chosen proportional to some experimental measure of
confidence. The second method allows more flexibility in choosing the
location and number of beams in the merge.

Once the form factor has been determined on the fundamental period of the
centered rectangular sublattice, the data can be extended over the fundamental
period of the doubled lattice as shown in figure 4. Finally, the results of
section 3.5 can be applied to transform from the form factor to the excitation
matrix α'_{nm}.

5.0 SIMULATION FLOW

The computer simulation, outlined in the flow charts of figures 7 and 8,
implements the theory of the preceding sections and provides a means for
testing various aspects of the spectral merge process. Figure 7 illustrates
the steps in obtaining the simulated near-field data which will be used for
the merged-spectrum analysis. The procedure of figure 8 uses the near-field
data for each of the steered beams to calculate the broadside-beam excitation
matrix from the merged spectrum. Implementation of the blocks in figure 8
will be completed in the next phase of the study. The final result depicted
in figure 8 should be the array excitation matrix input initially into the
simulation process of figure 7. Any differences are due to measurement errors
and effects of the merged-spectrum technique. Through simulation, we can
determine the most critical errors and the limits of accuracy.

5.1 Array Model

The array used in the simulation is shown schematically in figure 9. The
4350 active elements are arranged in 79 columns and 141 rows (in a nearly

14

circular region) on a centered rectangular lattice as shown in figures 1 and 9. To gain the convenience of working with a rectangular lattice, we add a virtual element between each actual element along the columns as shown in figures 3 and 10. Since virtual elements are assigned 0 amplitude in the excitation matrix, the performance of the array is not altered. Nominal element spacings in this doubled array are $a' = 0.5\lambda$ in the x direction (between columns) and $b' = 0.3\lambda$ in the y direction (between rows), resulting in an aperture approximately 42λ in diameter; however, spacing can be changed, as desired. The array is further extended with virtual elements (zero filling) so that it is rectangular in shape with $P \geq 79$ columns and $Q \geq 141$ rows. Efficient use of the FFT dictates that P and Q should be powers of 2; for example, $P = 128$, $Q = 256$.

5.2 Simulation Examples

The first simulation example is for a broadside beam with no errors in any of the elements. Figures 11 through 14 are center line (x = 0 and y = 0) plots of the excitation matrix along with the corresponding field amplitude on measurement planes at 20 cm and 50 cm. The field amplitudes, which are normalized to 0 dB peak, were calculated using eq (13). (The frequency is 3 GHz for all computations.)

The broadside-beam array (form) factor was calculated using eq (30) with $P = Q = 512$ and results are shown in figures 15 through 18. Figures 15 and 16 are plots of the array factor over the fundamental period of the doubled lattice: $-1 < k_x/k \leq 1$, $-5/3 < k_y/k \leq 5/3$. These figures confirm that the fundamental period for the doubled array can be determined if the array factor is known in the subregion (shaded in fig. 4) which corresponds to the fundamental period of the actual array without virtual elements. (See the discussion of fig. 4 in section 3.3.) Thus "doubling" of the array, which is done for computational convenience, does not cost anything from a measurement point of view. Figures 17 and 18 show the array factor in the principal planes. [The horizontal bands in the array factor evident in figure 15 apparently arise because the elements are driven pairwise in the y direction (fig. 12). Similar vertical bands might be expected in figure 15, as well, except that the y = 0 row (the excitations are plotted in fig. 11) is the only row with elements driven in pairs.]

The next step in the simulation is the calculation of the measured data on a specified measurement plane. The array factor is first multiplied by the

coupling product between probe and average element patterns and then by the factor $\exp(i\gamma z_0)$ before transforming to the near-field with the FFT [see eq (13)]. A typical spectrum for both the probe and element is shown in figures 19 and 20 with the amplitude of the coupling product $D^e(\hat{\mathbf{k}})$ shown in figure 21. Since both the probe and element have very broad patterns, they have little effect on the spectrum of the low sidelobe array. (The major effect occurs when $K/k > 0.6$ where the coupling product is reduced by 10 to 30 dB due to the combined effect of probe and element patterns.) The factor $\exp(i\gamma z_0)$ is important, however. Within the visible region (fig. 22), where γ is real, it reflects the phase progression of plane waves propagating from the aperture to the measurement plane. Beyond the visible region (fig. 23), where γ is imaginary, it reflects the exponential attenuation of the evanescent components of the spectrum.

Figures 24 through 27 represent error-free data from an open-ended waveguide probe on measurement planes 20 cm and 50 cm from the aperture of an array with no faulty or misaligned elements. The program provides the option of introducing various errors and example array factors are shown in figures 28 through 31. Here, the excitation phases have been modified, by adding a sinusoidal error in the x and/or y directions, to produce paired error lobes in addition to the main beam. Other errors will be simulated in future studies.

In addition to the broadside beams illustrated thus far, steered beams can be produced by imposing a linearly varying phase on the excitation matrix (section 3.2). An example array factor is shown in figure 32. The array factor for a steered beam can be obtained by translating the form factor (fig. 15) as indicated by eq (17). Multiple beam directions are required for the merged-spectrum simulation.

6.0 SUMMARY

Computer code and supporting analysis have been developed as the basis for a thorough evaluation by simulation of the merged-spectrum technique for aligning planar arrays. The actual evaluation of the merged-spectrum technique will be described in a future report.

REFERENCES

[1]   Patton, W.T.   Phased array alignment with planar near-field scanning; or determining element excitation from planar near-field data.   In Proc. Antenna Appl. Symp., Univ. Illinois; Sept. 1981.

[2]   Kerns, D.M.   Plane-wave scattering-matrix theory of antennas and antenna-antenna interactions.   Nat. Bur. Stand. (U.S.) Monograph 162; June 1981.

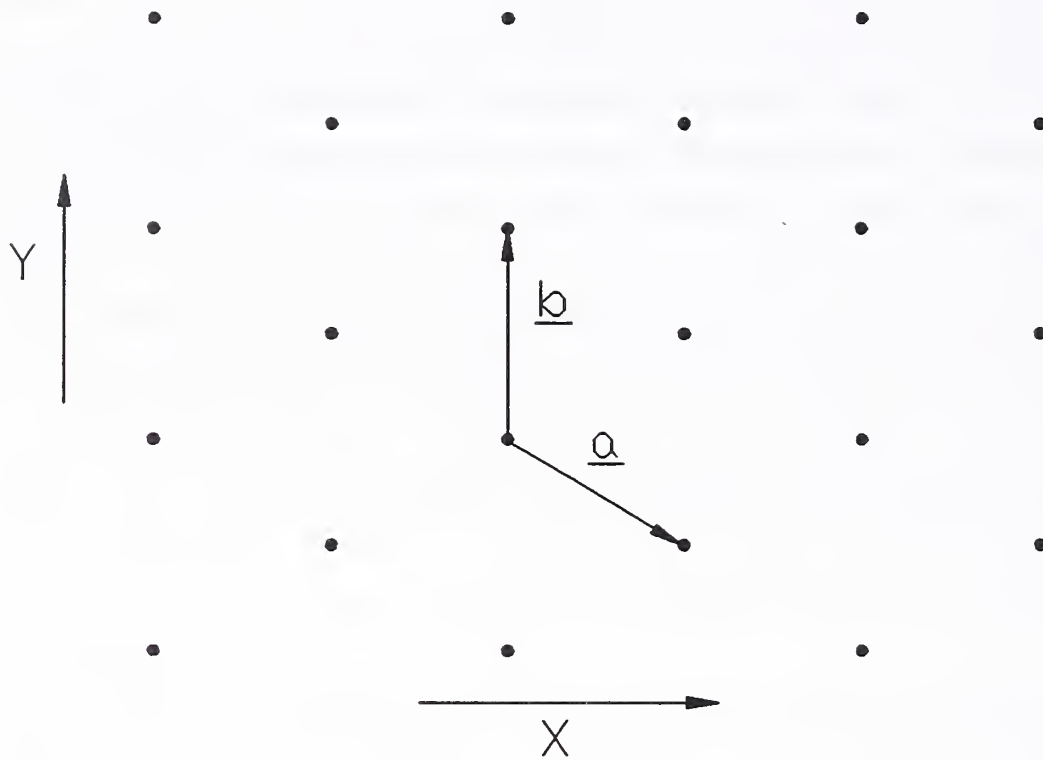[3]   Ma, M.T.   Theory and application of antenna arrays.   New York: Wiley; 1974.

Figure 1.   A centered rectangular lattice showing a set of fundamental (and primitive) lattice vectors. $\mathbf{a} = \lambda(1/2\ \hat{\mathbf{x}} - 3/10\ \hat{\mathbf{y}})$, $\mathbf{b} = \lambda\ 3/5\ \hat{\mathbf{y}}$.
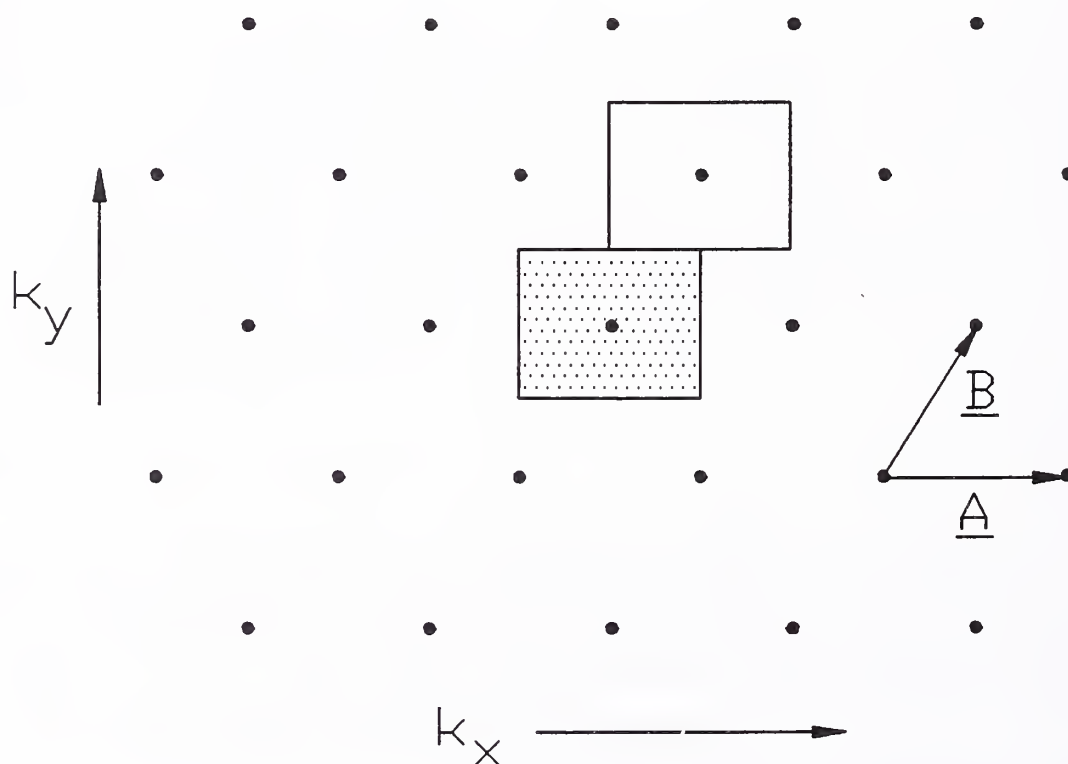
Figure 2.   The reciprocal lattice for the lattice of figure 1. $\mathbf{A} = 2k\ \hat{\mathbf{x}}$, $\mathbf{B} = k(\hat{\mathbf{x}} + 5/3\ \hat{\mathbf{y}})$.   If the array factor is known on the fundamental period (shaded), then it may be determined everywhere by periodic repetition.   For example, in the open rectangle $A(\mathbf{K}) = A(\mathbf{K} - \mathbf{B})$.
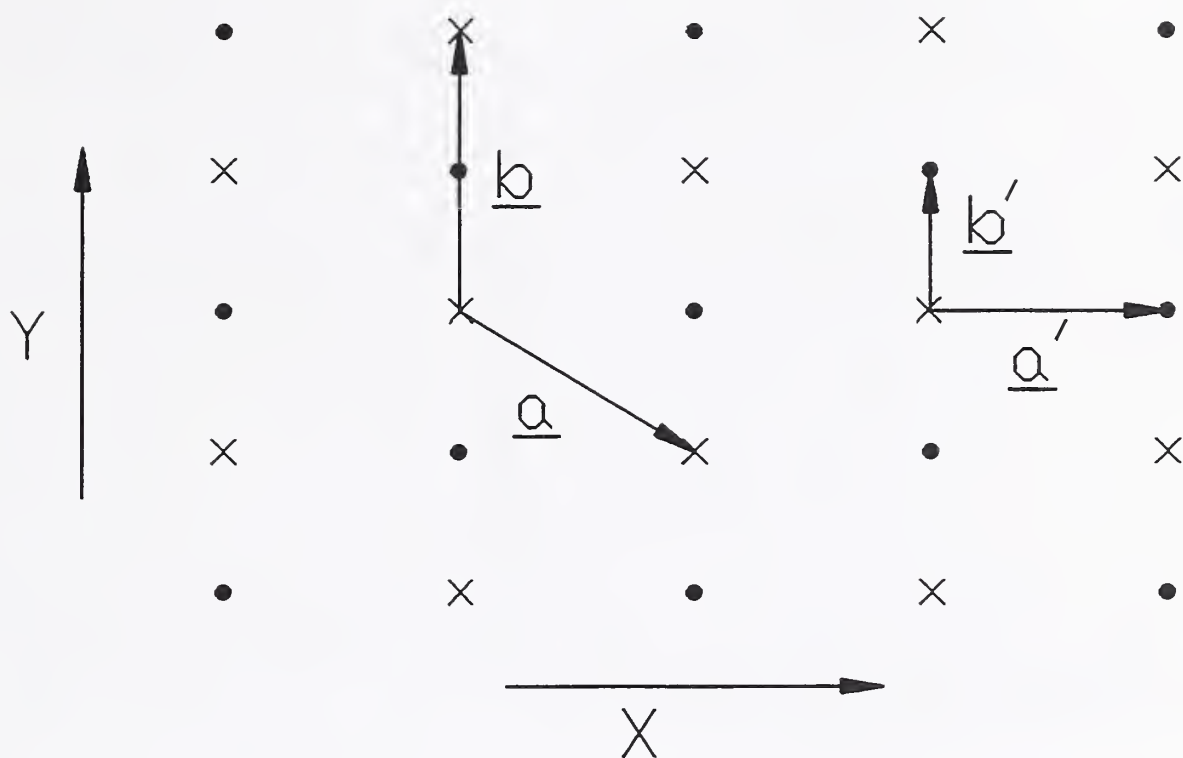
18

Figure 3. A rectangular lattice obtained from the centered rectangular lattice of figure 1 by adding interstitial points. $\mathbf{a}' = \lambda\ 1/2\ \hat{\mathbf{x}}$, $\mathbf{b}' = \lambda\ 3/10\ \hat{\mathbf{y}}$. Element positions are marked with x's. ($\alpha'_{nm} = 0$, n+m even.)
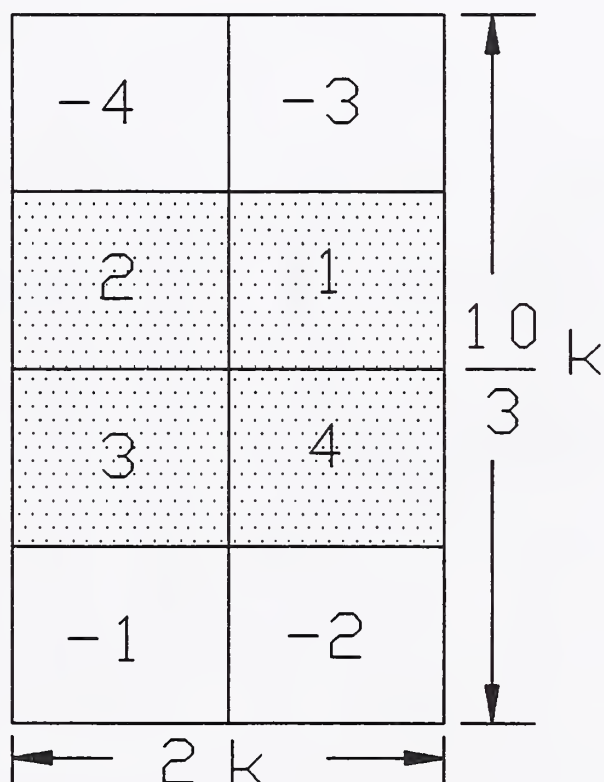

Figure 4. A fundamental period in the reciprocal lattice for the doubled lattice of figure 3. A(K) may be determined everywhere from its values on the fundamental period of the centered rectangular sublattice (shaded); The mapping is indicated by quadrant. The minus signs occur because the centered rectangular sublattice is offset from the origin.
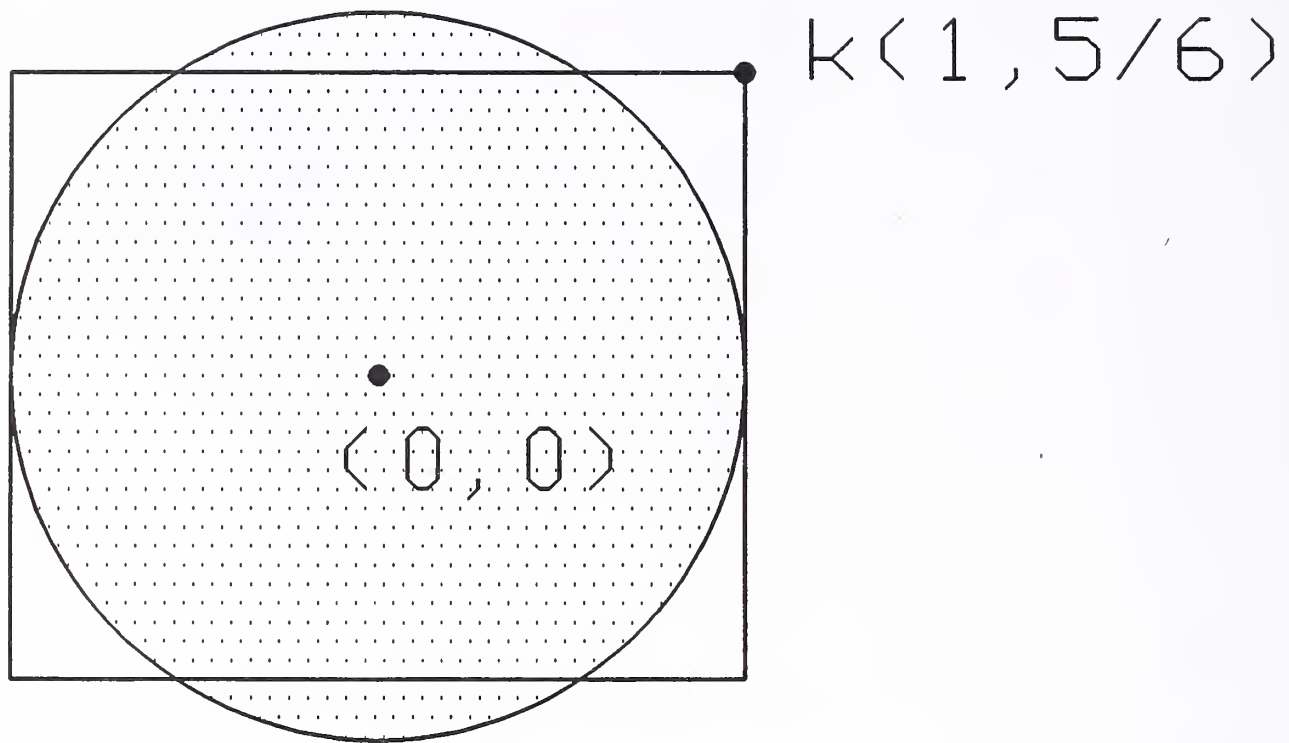
Figure 5. The visible region for a broadside beam is the shaded disk. Extrapolation would be necessary to determine the form factor from this information. In the merged-spectrum technique, direct measurement of the fundamental period (rectangle) is accomplished via beam steering.
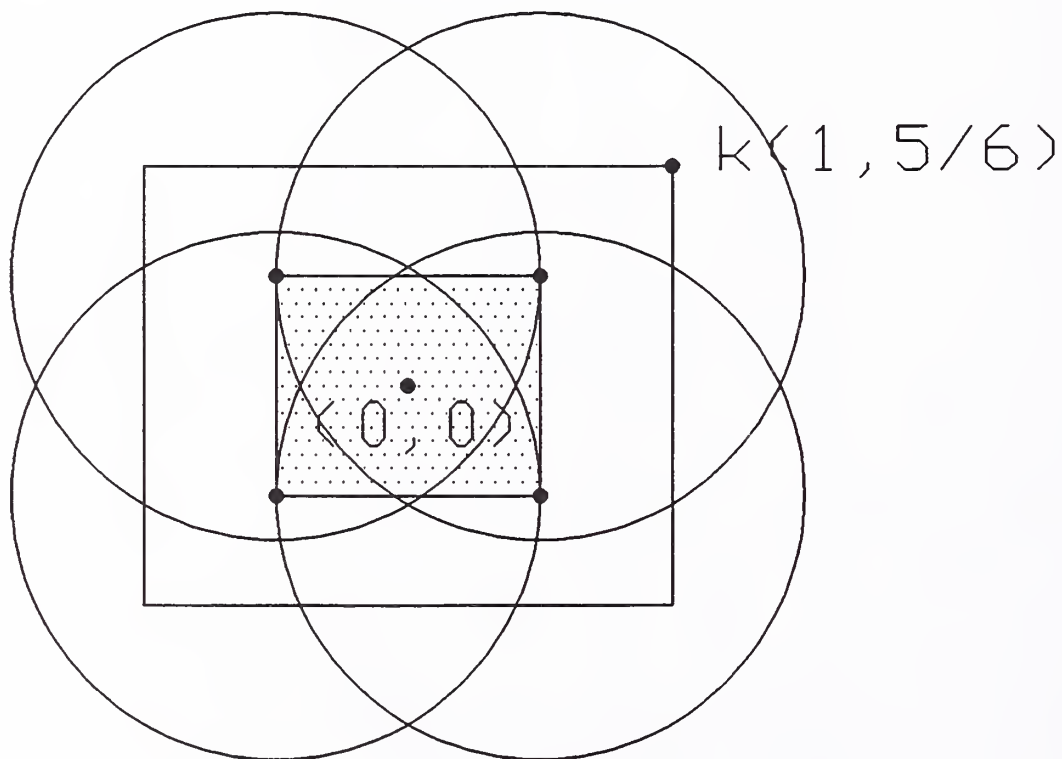

Figure 6. When the beam is steered to the four locations $K_0 = k(\pm 1/2\ \hat{x}\ \pm 5/12\ \hat{y})$ marked with •'s, the entire fundamental period can be measured directly. The visible region corresponding to each beam direction is indicated by a circle. The shaded rectangle ($\theta \leq 40.60°$) is the smallest region in which coupling products must be determined.
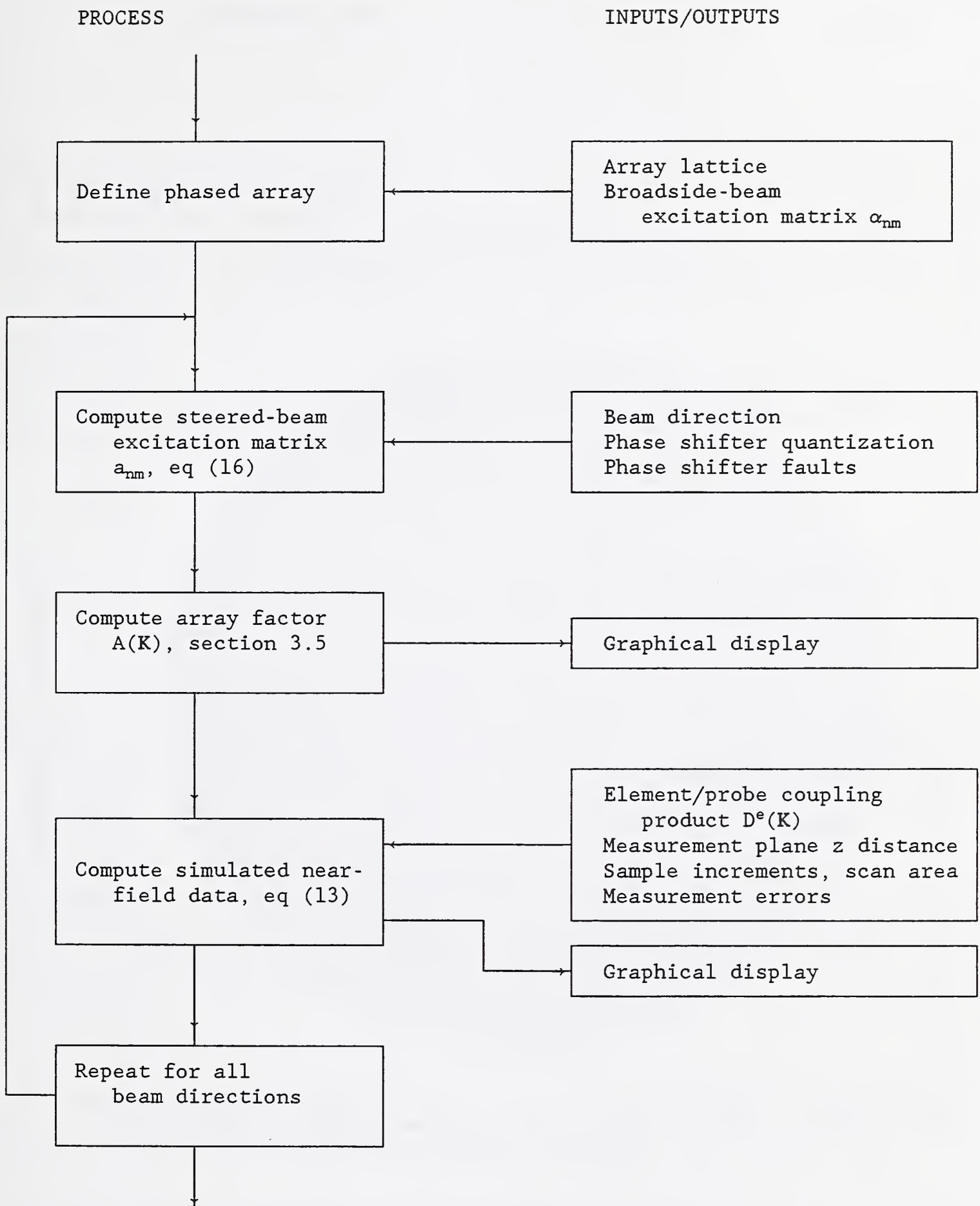
PROCESS   INPUTS/OUTPUTS

┌─────────────────────────┐   ┌────────────────────────────────┐
│   │   │ Array lattice   │
│ Define phased array   │◄─────────│ Broadside-beam   │
│   │   │   excitation matrix α_{nm} │
└─────────────────────────┘   └────────────────────────────────┘

┌─────────────────────────┐   ┌────────────────────────────────┐
│ Compute steered-beam   │   │ Beam direction   │
│   excitation matrix   │◄─────────│ Phase shifter quantization   │
│ a_{nm}, eq (16)   │   │ Phase shifter faults   │
└─────────────────────────┘   └────────────────────────────────┘

┌─────────────────────────┐   ┌────────────────────────────────┐
│ Compute array factor   │   │   │
│   A(K), section 3.5   │─────────►│ Graphical display   │
│   │   │   │
└─────────────────────────┘   └────────────────────────────────┘

┌─────────────────────────┐   ┌────────────────────────────────┐
│   │   │ Element/probe coupling   │
│   │   │   product $D^e(K)$ │
│ Compute simulated near- │◄─────────│ Measurement plane z distance   │
│   field data, eq (13) │   │ Sample increments, scan area   │
│   │   │ Measurement errors   │
│   │   └────────────────────────────────┘
│   │   ┌────────────────────────────────┐
│   │─────────►│ Graphical display   │
└─────────────────────────┘   └────────────────────────────────┘

┌─────────────────────────┐
│ Repeat for all   │
│   beam directions   │
│   │
└─────────────────────────┘

Figure 7. Block diagram showing the phased-array simulation and the near-
field measurement simulation.

21

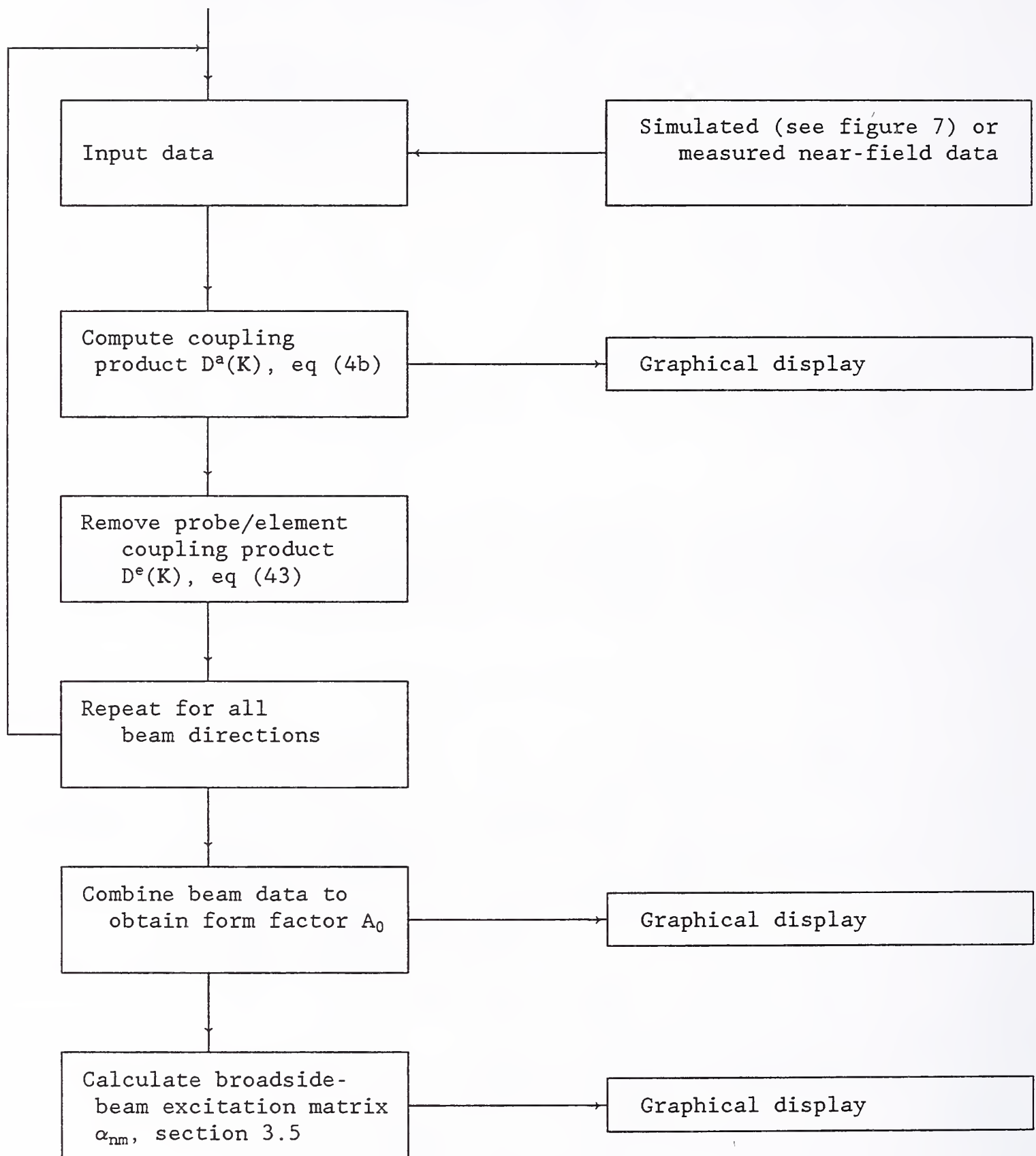PROCESS   INPUTS/OUTPUTS

```
┌─────────────────────┐          ┌────────────────────────────────┐
│                     │          │  Simulated (see figure 7) or   │
│  Input data         │◄─────────│  measured near-field data      │
│                     │          │                                │
└─────────────────────┘          └────────────────────────────────┘

┌─────────────────────┐          ┌────────────────────────────────┐
│  Compute coupling   │          │                                │
│   product Dᵃ(K), eq (4b) │────►│  Graphical display             │
│                     │          │                                │
└─────────────────────┘          └────────────────────────────────┘

┌─────────────────────┐
│  Remove probe/element │
│   coupling product  │
│   Dᵉ(K), eq (43)    │
└─────────────────────┘

┌─────────────────────┐
│  Repeat for all     │
│   beam directions   │
└─────────────────────┘

┌─────────────────────┐          ┌────────────────────────────────┐
│  Combine beam data to │        │                                │
│   obtain form factor A₀ │────►│  Graphical display             │
│                     │          │                                │
└─────────────────────┘          └────────────────────────────────┘

┌─────────────────────┐          ┌────────────────────────────────┐
│  Calculate broadside- │        │                                │
│   beam excitation matrix │───►│  Graphical display             │
│   αₙₘ, section 3.5  │          │                                │
└─────────────────────┘          └────────────────────────────────┘
```

Process blocks:

- Input data
- Compute coupling product $D^a(K)$, eq (4b)
- Remove probe/element coupling product $D^e(K)$, eq (43)
- Repeat for all beam directions
- Combine beam data to obtain form factor A_0
- Calculate broadside-beam excitation matrix α_{nm}, section 3.5

Inputs/Outputs:

- Simulated (see figure 7) or measured near-field data
- Graphical display
- Graphical display
- Graphical display

Figure 8. Block diagram showing the merged-spectrum technique for determining the phased-array excitation matrix.

ACTUAL ELEMENTS IN ARRAY
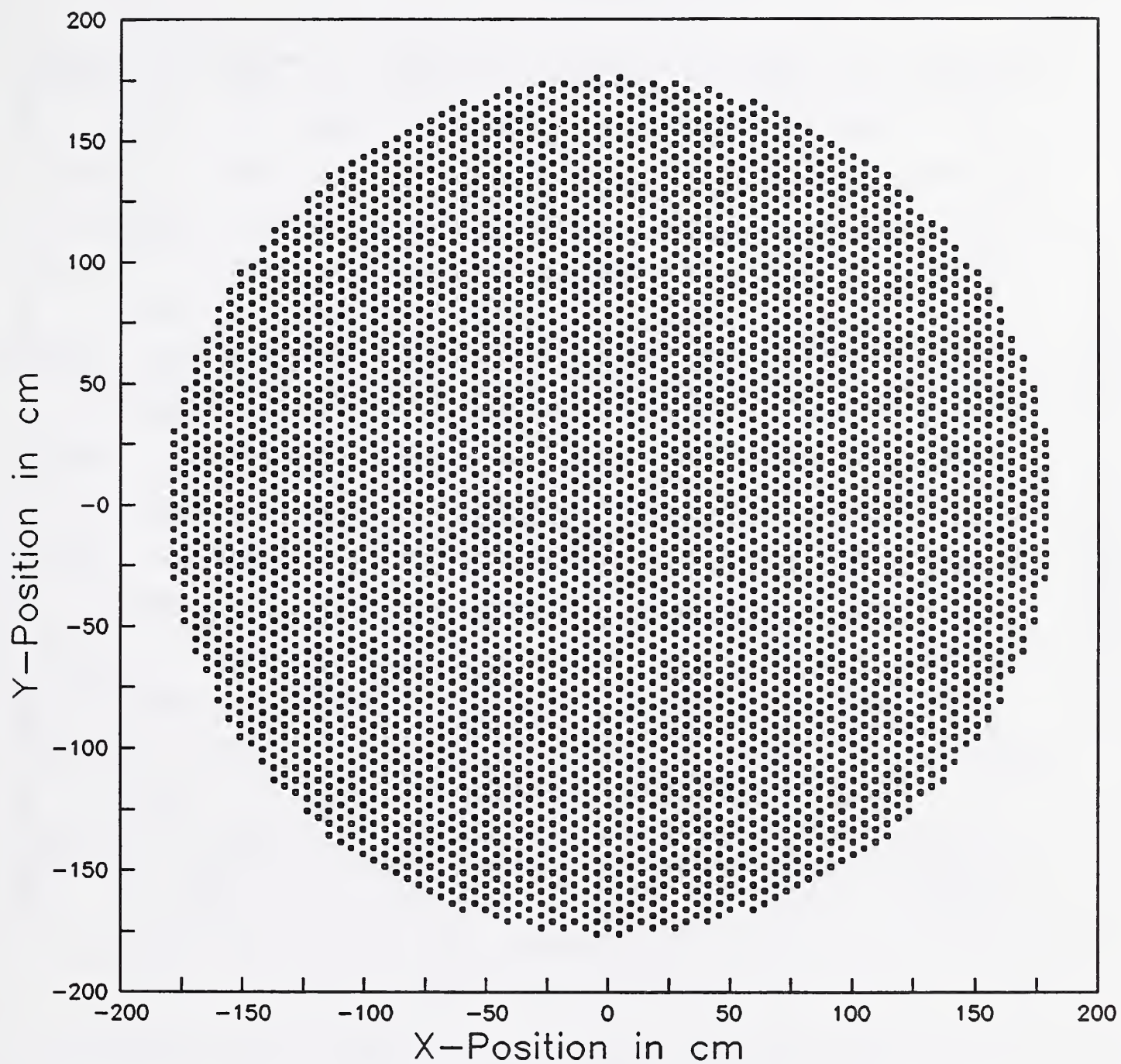
Figure 9. Schematic of the phased array showing location of active elements.
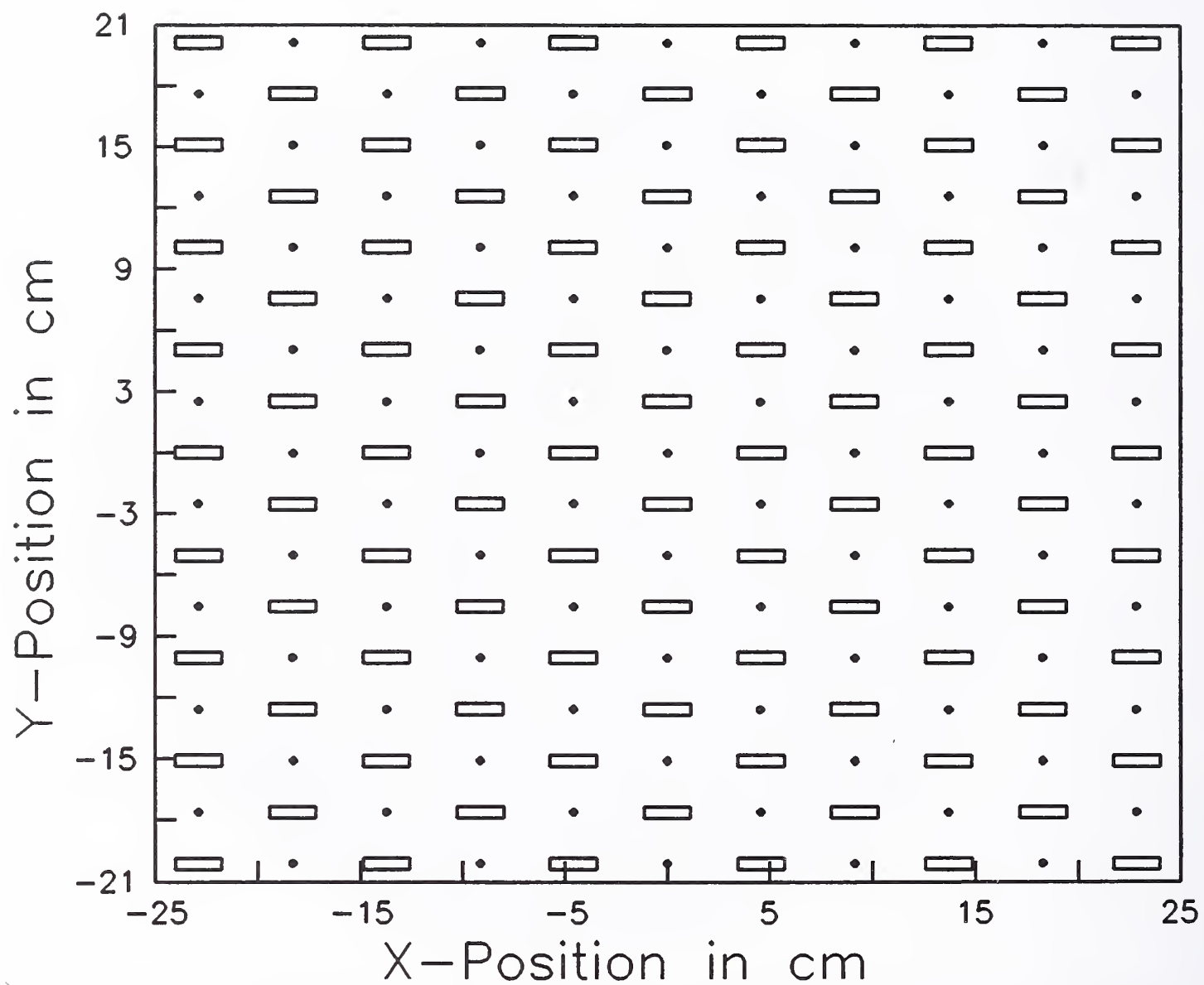
Figure 10. Schematic of the central part of the phased array showing the location of active elements (▫) and virtual elements (•).
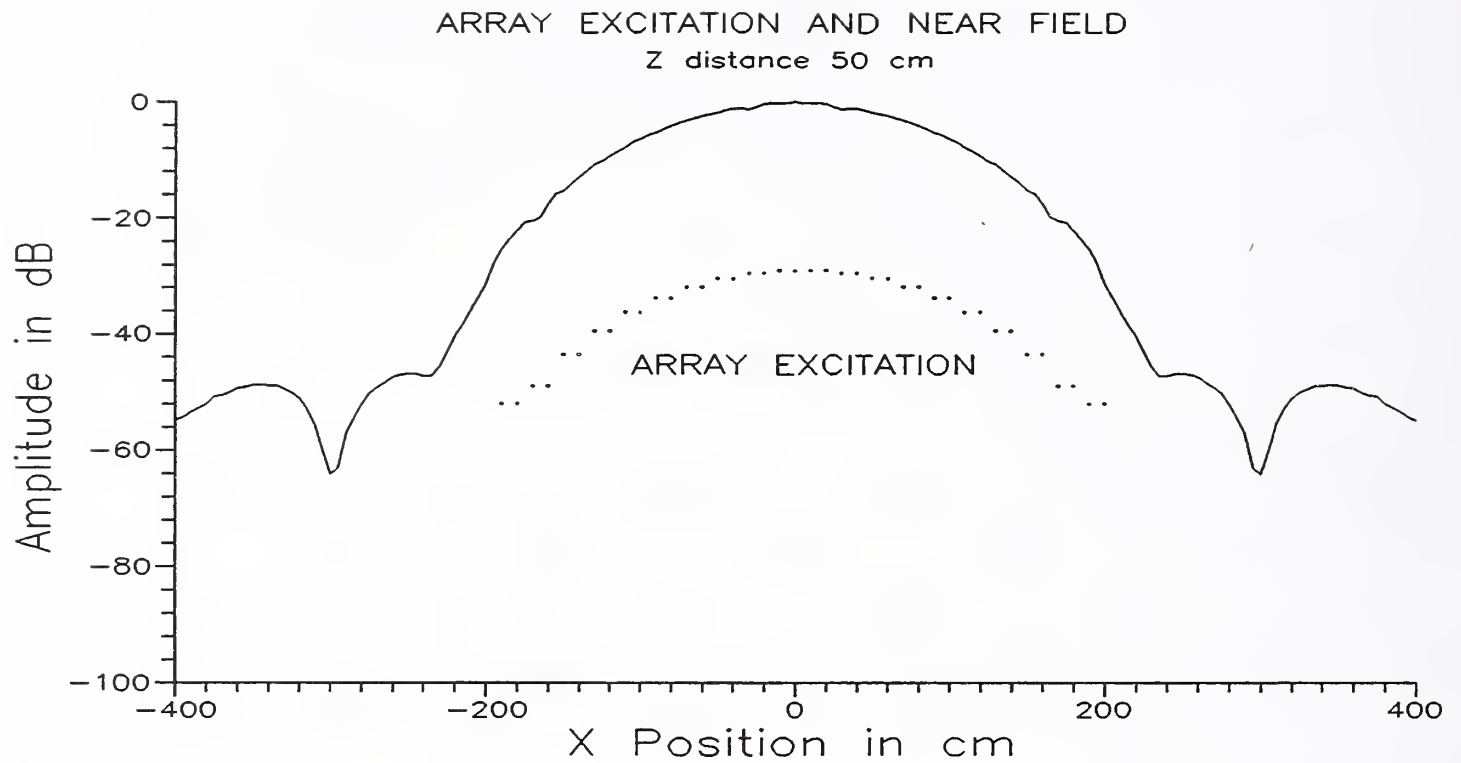
ARRAY EXCITATION AND NEAR FIELD
Z distance 20 cm
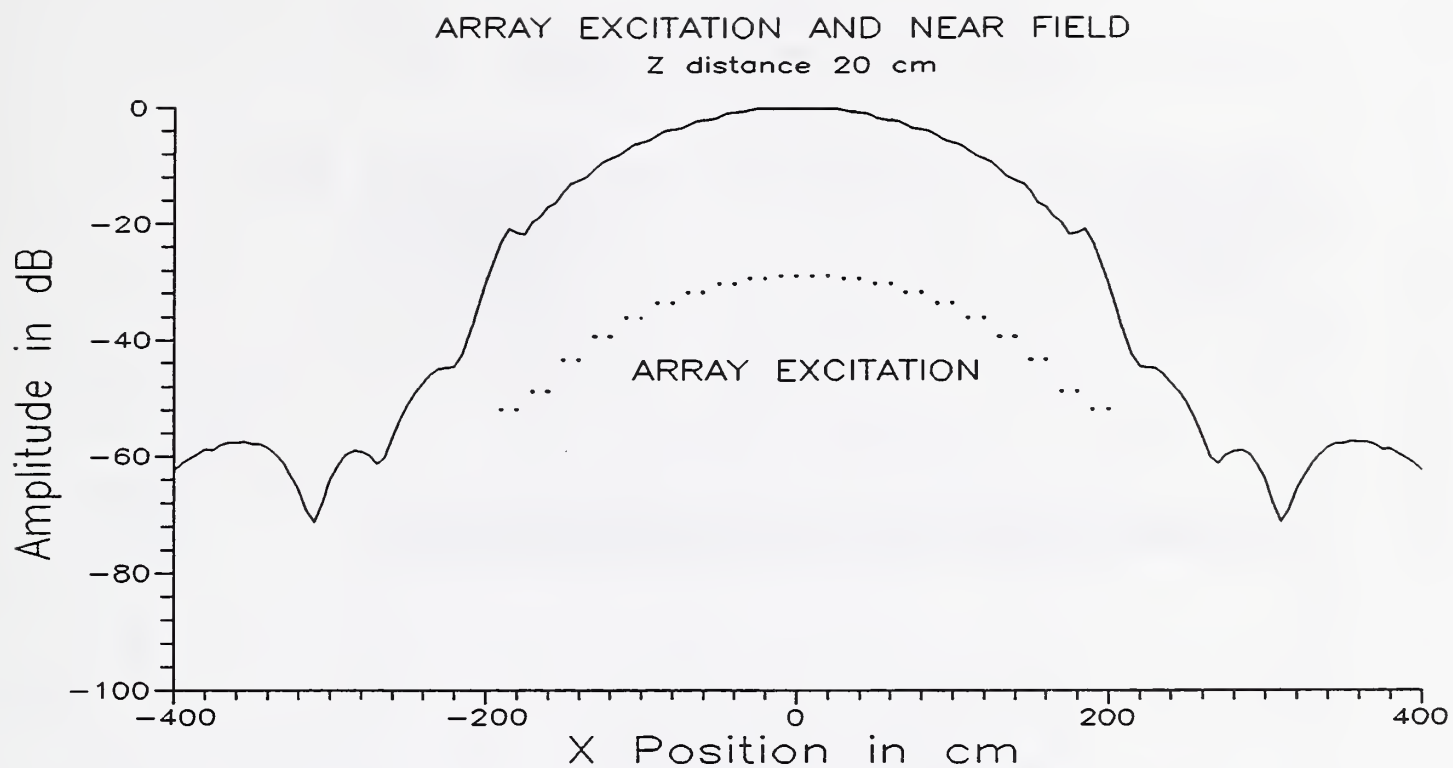
Figure 11. Relative amplitude excitations (dots) of elements along the center
row, y = 0, and field amplitude (solid line), normalized to 0 dB peak,
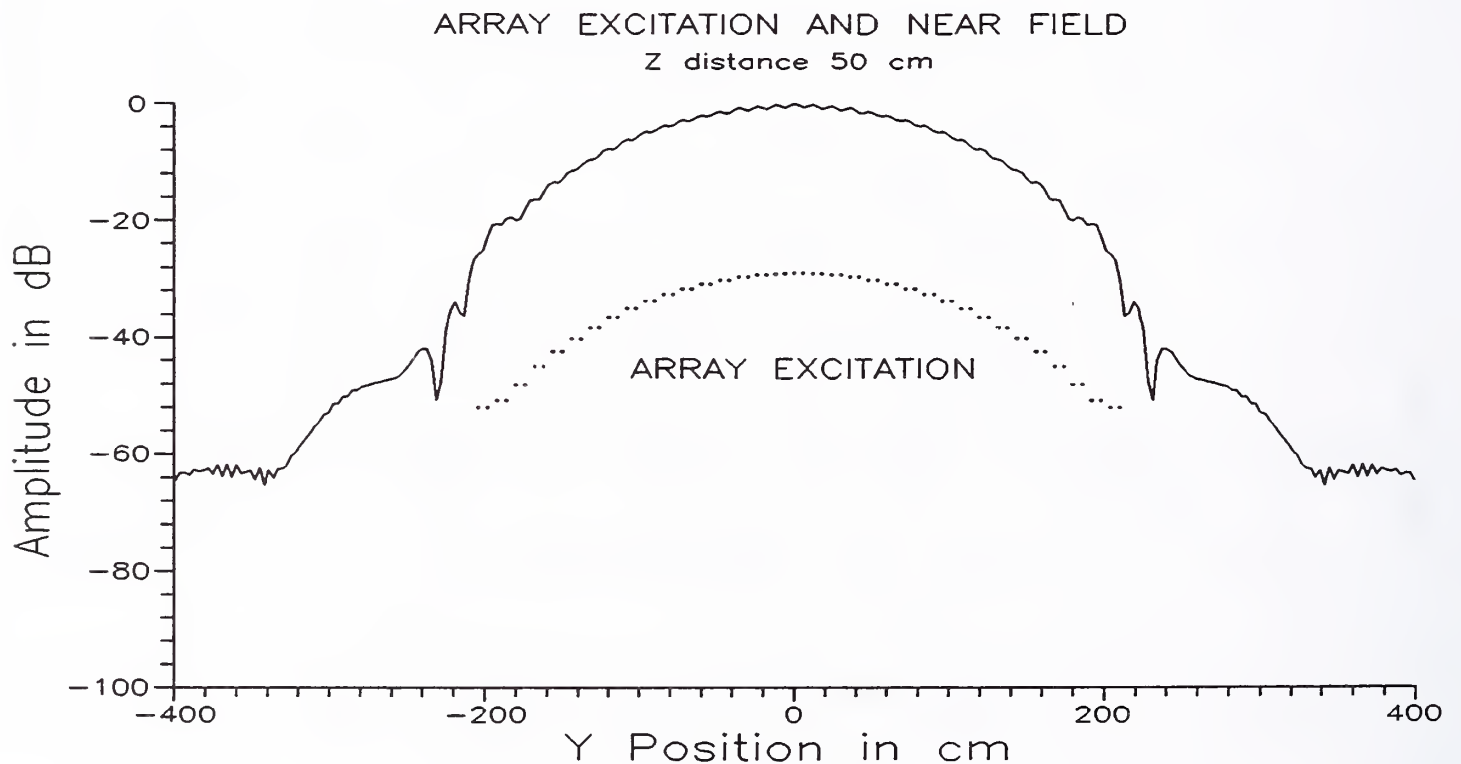at z = 20 cm. Frequency is 3 GHz.

ARRAY EXCITATION AND NEAR FIELD
Z distance 20 cm
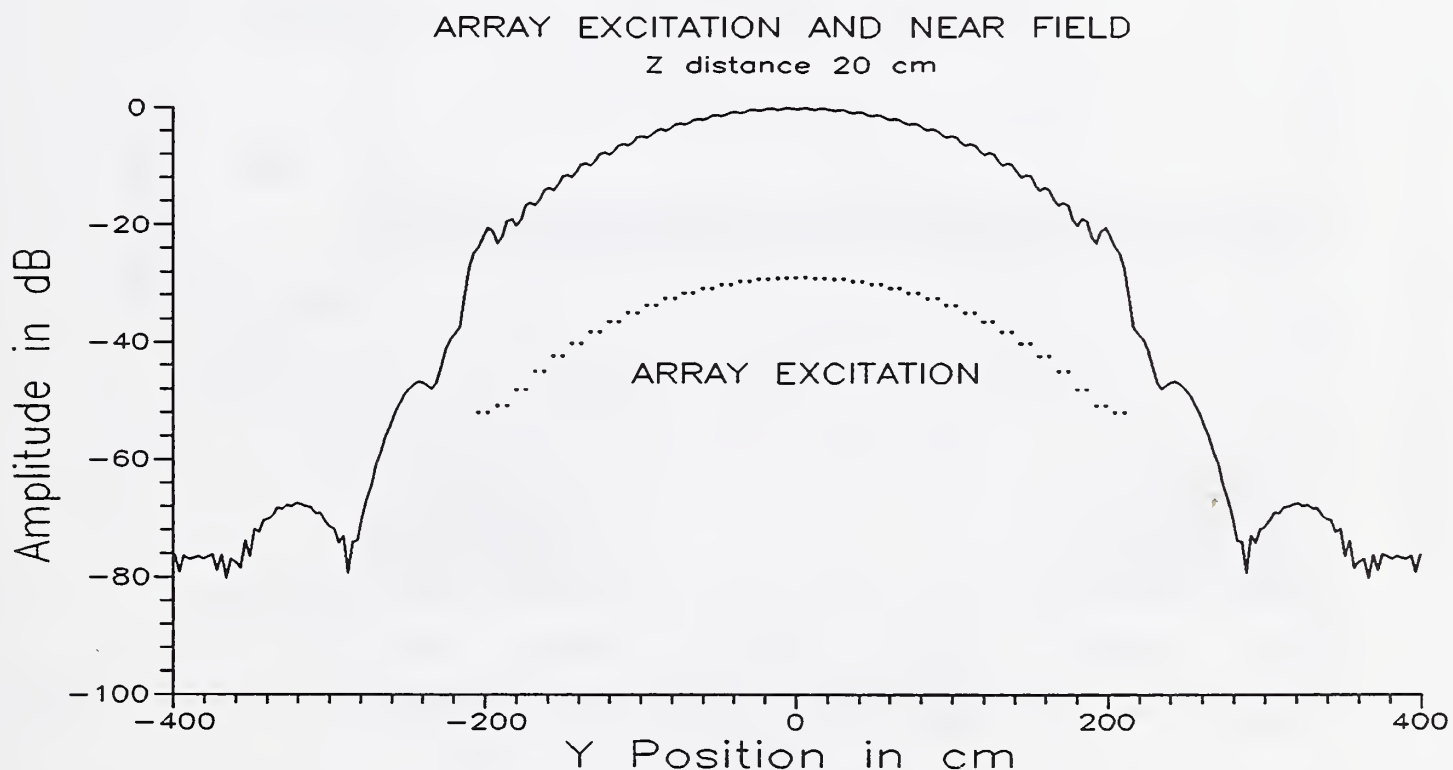
Figure 12. Relative amplitude excitations (dots) of elements along the center
column, x = 0, and field amplitude (solid line), normalized to 0 dB
peak, at z = 20 cm. Frequency is 3 GHz.

ARRAY EXCITATION AND NEAR FIELD
Z distance 50 cm

Figure 13. Relative amplitude excitations (dots) of elements along the center
row, y = 0, and field amplitude (solid line), normalized to 0 dB peak,
at z = 50 cm. Frequency is 3 GHz.

ARRAY EXCITATION AND NEAR FIELD
Z distance 50 cm

Figure 14. Relative amplitude excitations (dots) of elements along the center
column, x = 0, and field amplitude (solid line), normalized to 0 dB
peak, at z = 50 cm. Frequency is 3 GHz.

10 dB Contours (0, −60)
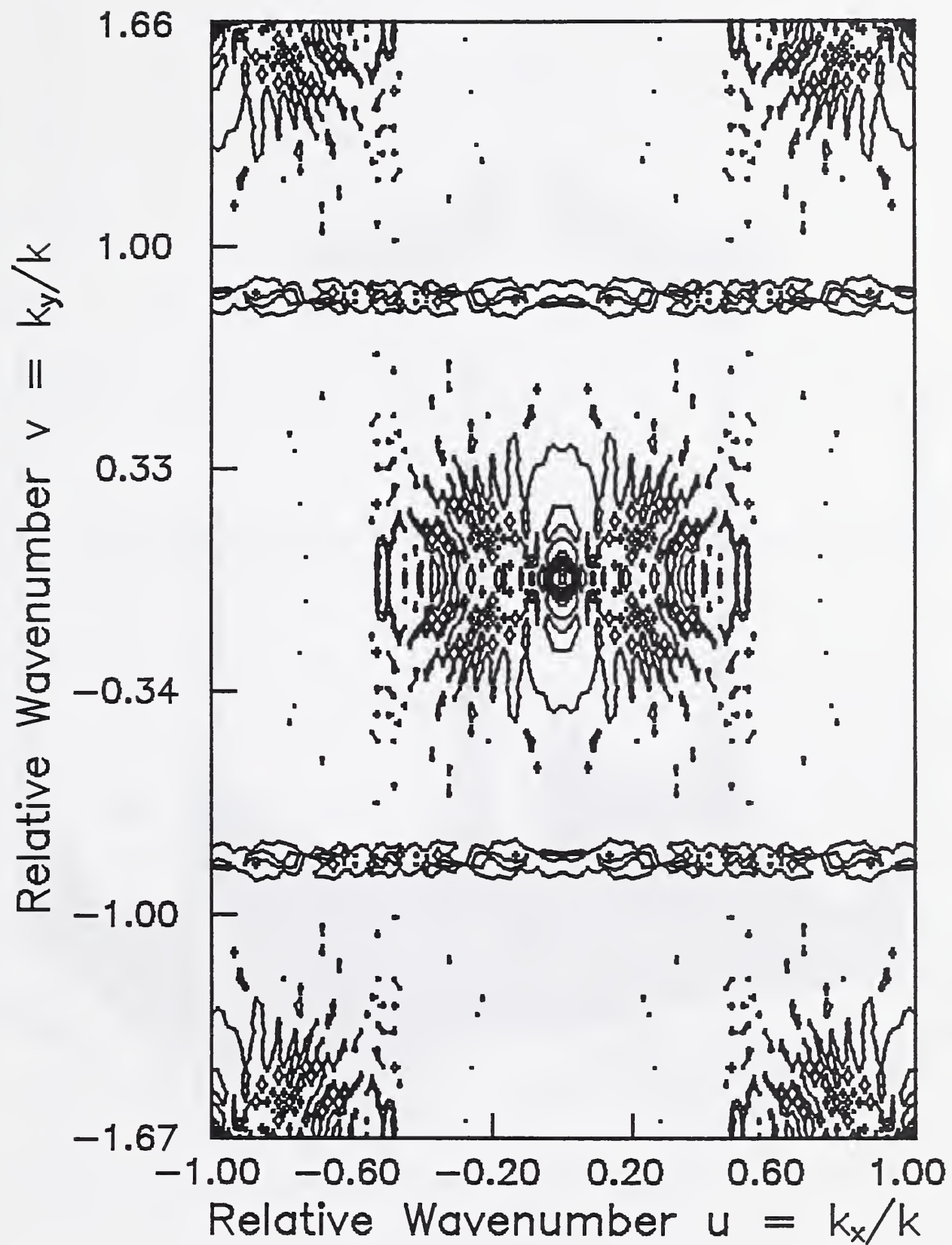
Figure 15. Contour plot of the array factor for the doubled array composed of active and virtual elements.
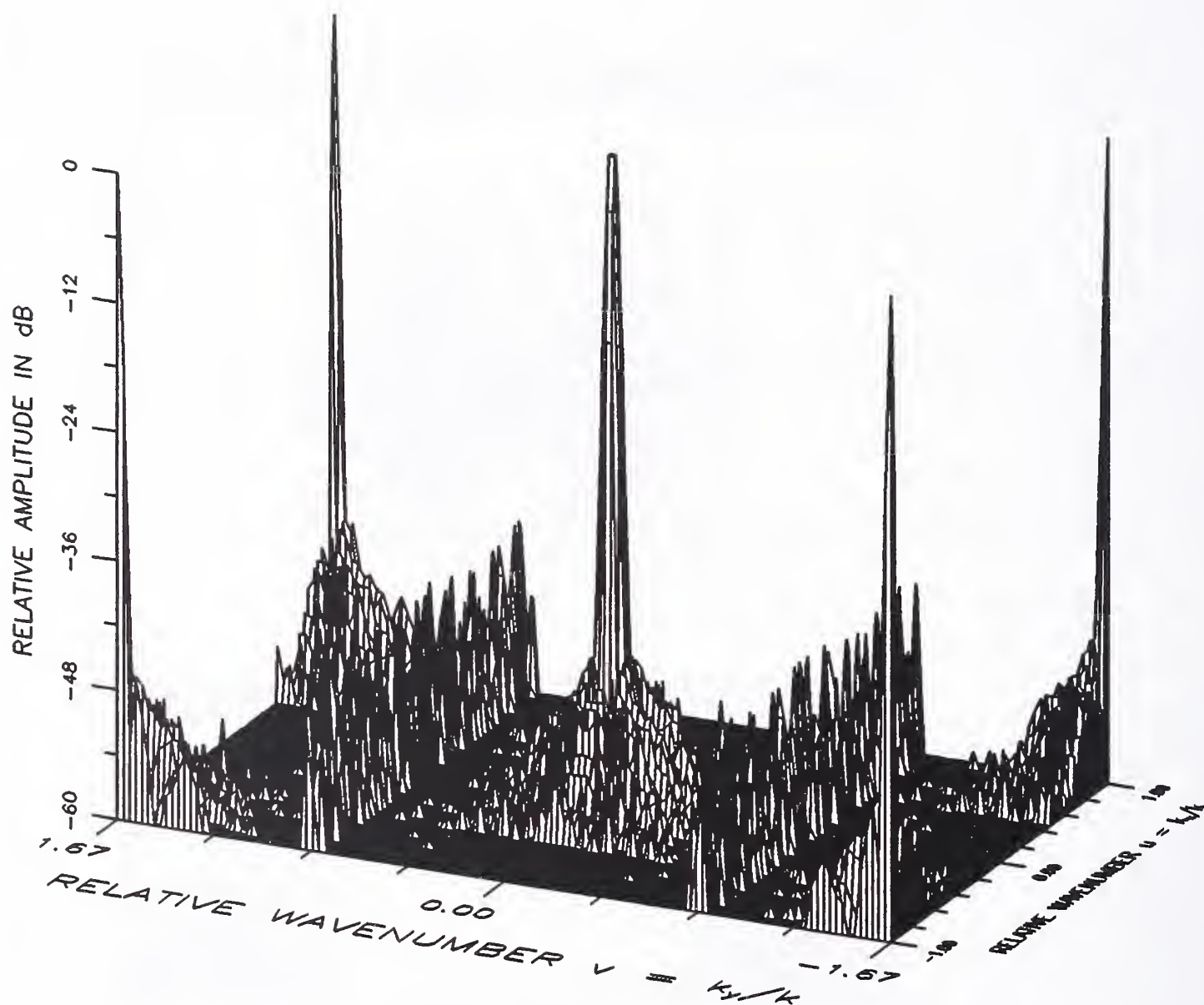
Figure 16. Perspective plot of the array factor for the doubled array composed of active and virtual elements.
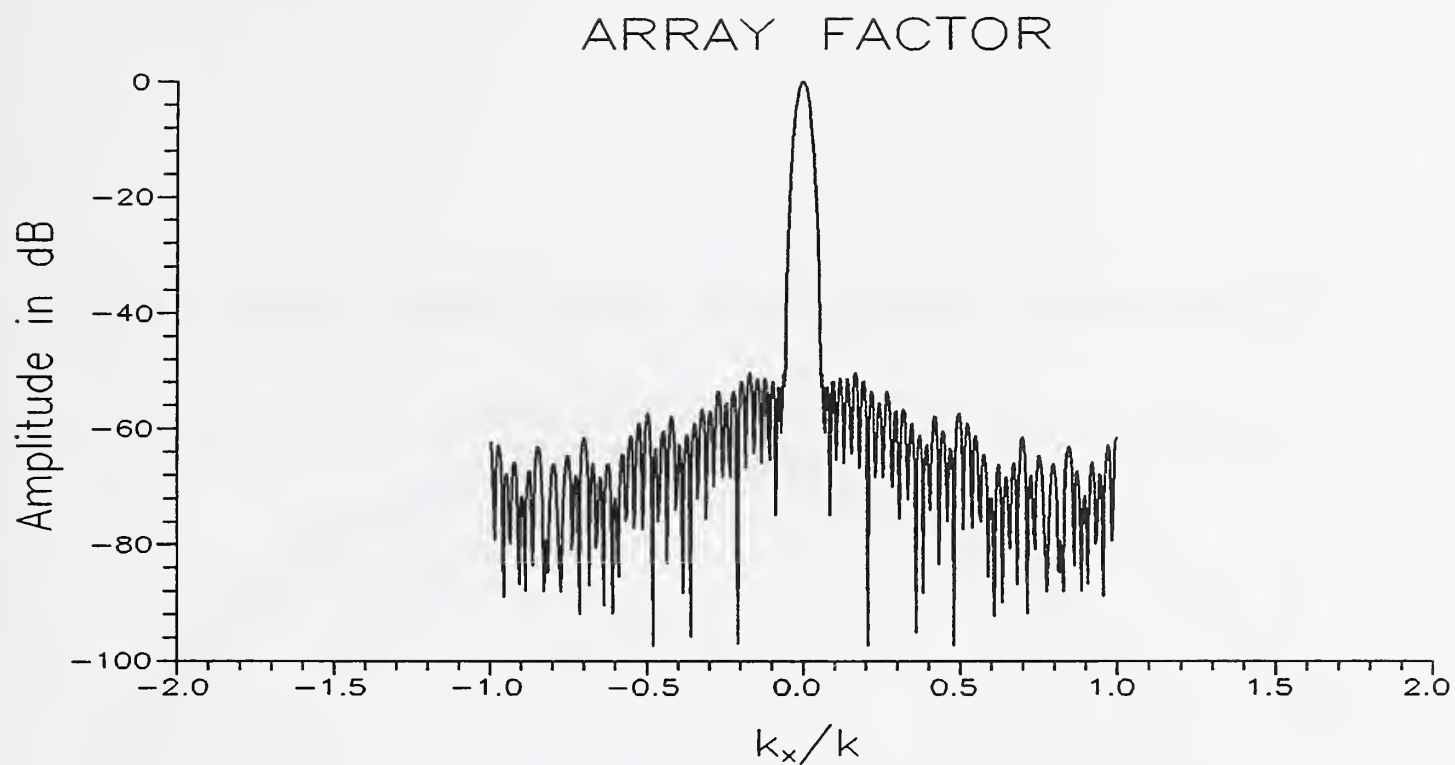
ARRAY FACTOR

Figure 17. Principal plane ($k_y = 0$) cut of the array factor for the doubled array composed of active and virtual elements.
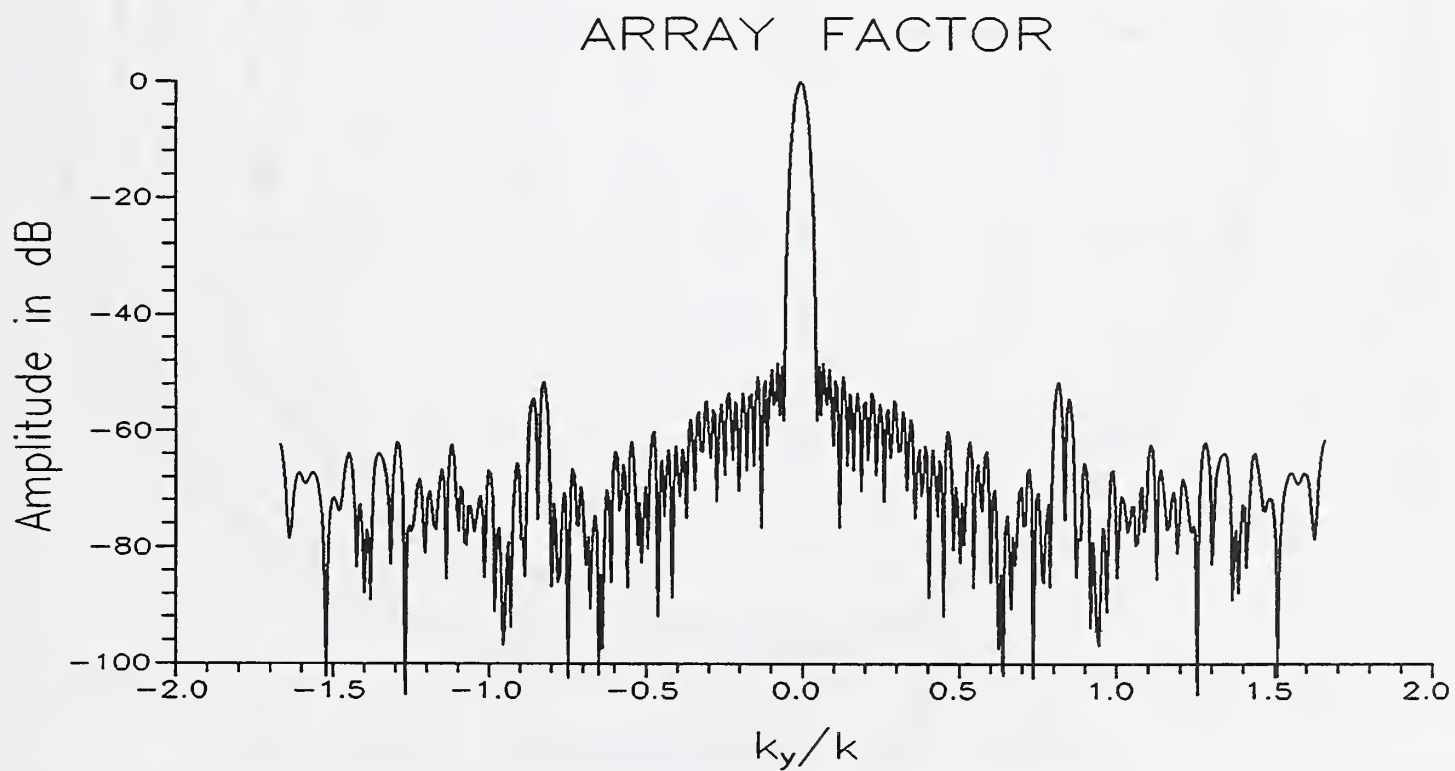
ARRAY FACTOR

Figure 18. Principal plane ($k_x = 0$) cut of the array factor for the doubled array composed of active and virtual elements.

29

OPEN-END WAVEGUIDE SPECTRUM, AMPLITUDE

2 dB CONTOURS (0, -20)
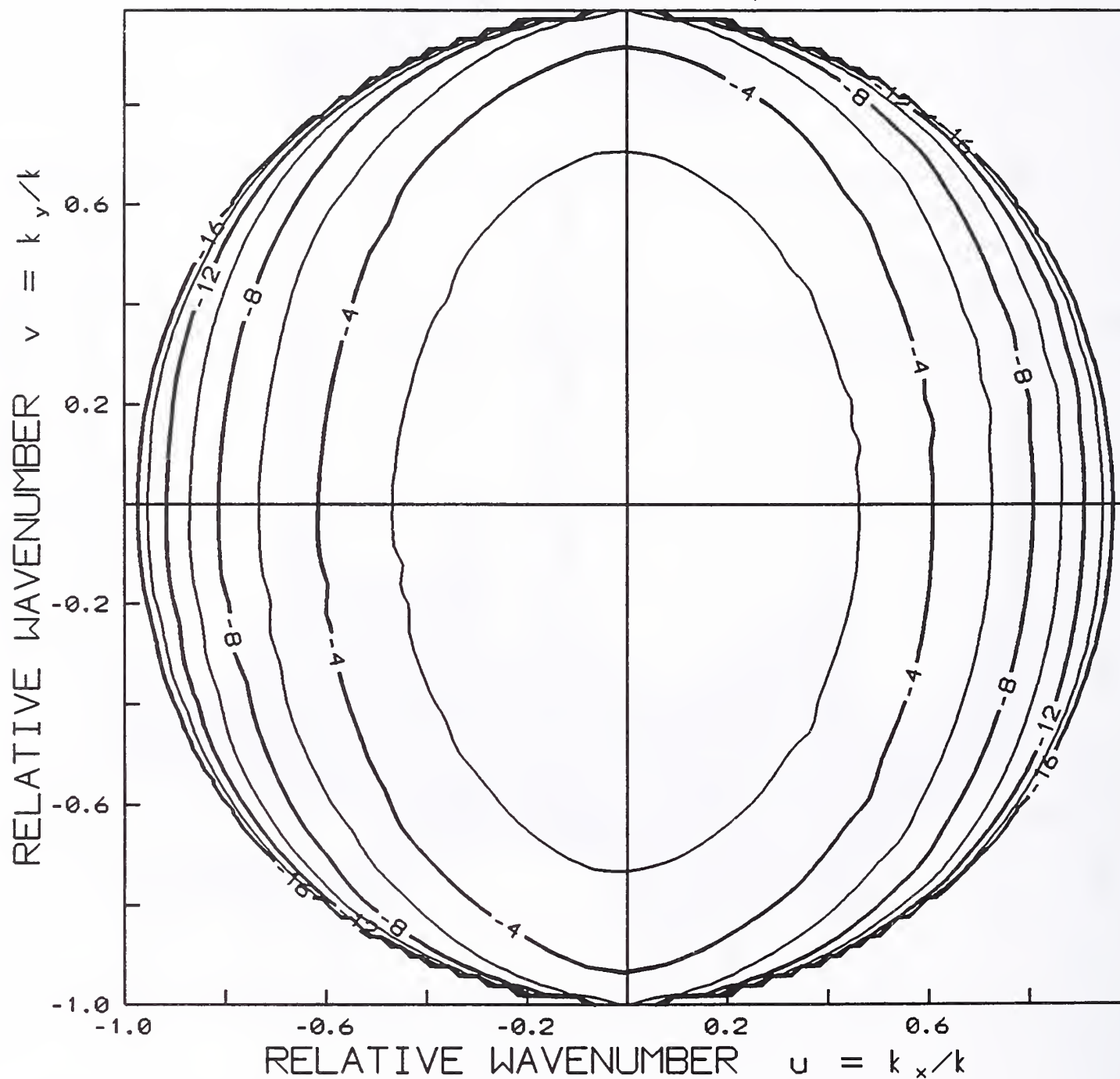
Figure 19. Contour plot of the probe's receiving pattern, amplitude for open-ended waveguide.
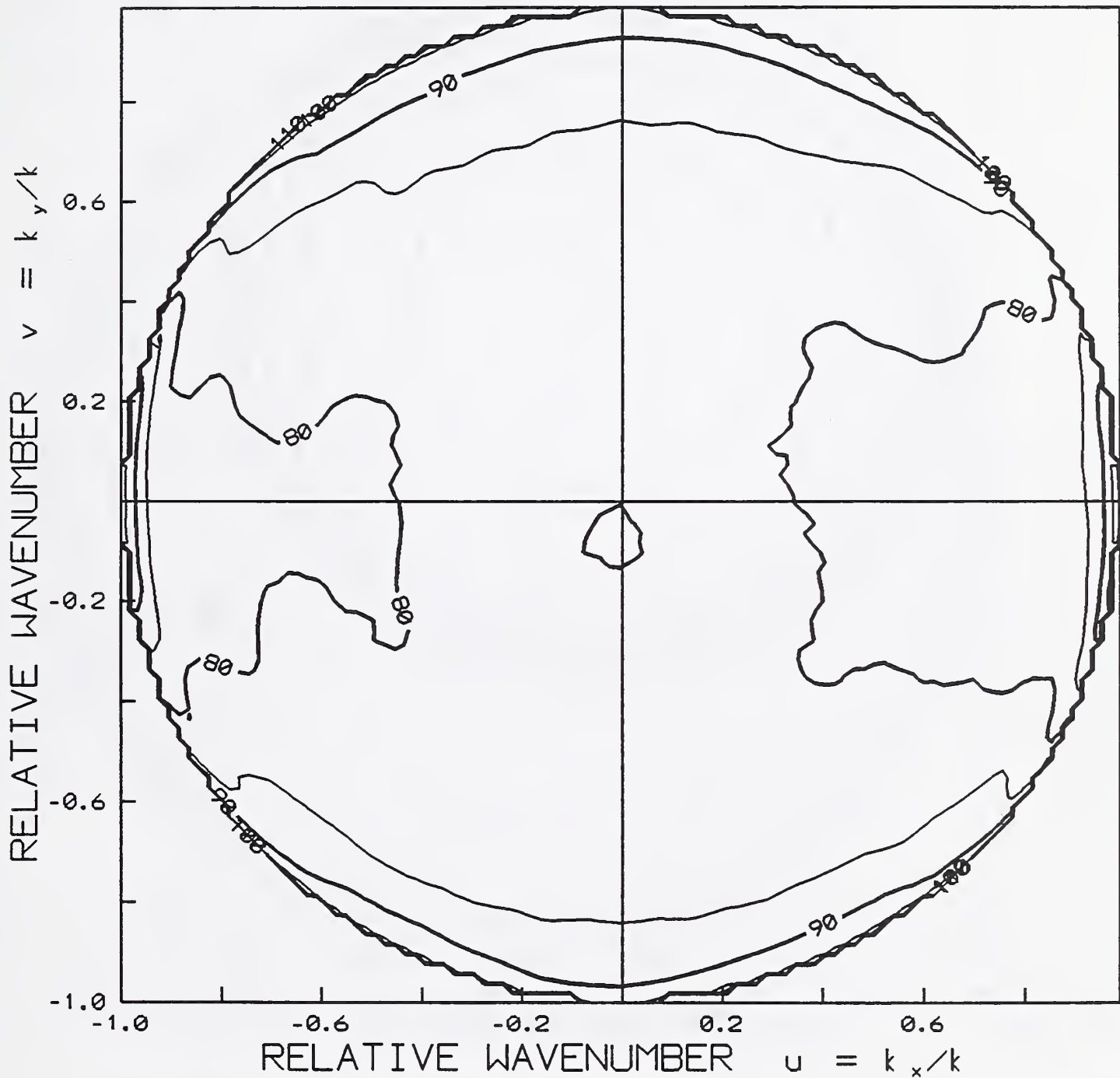
Figure 20. Contour plot of the probe's receiving pattern, phase for open-ended waveguide.
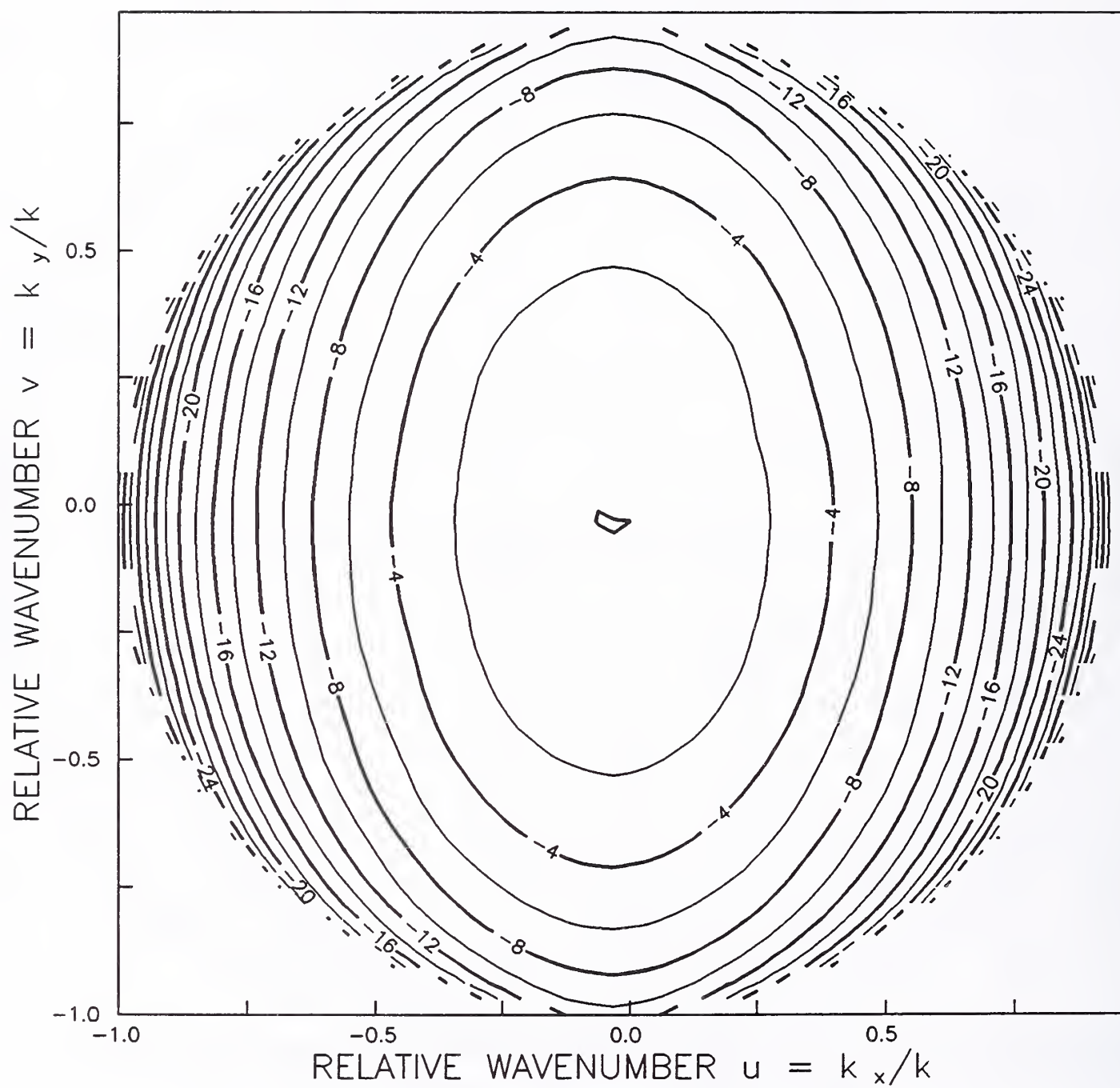
Figure 21. Amplitude of the coupling product $D^e(\hat{k})$ assuming probe and average element are open-ended waveguides.
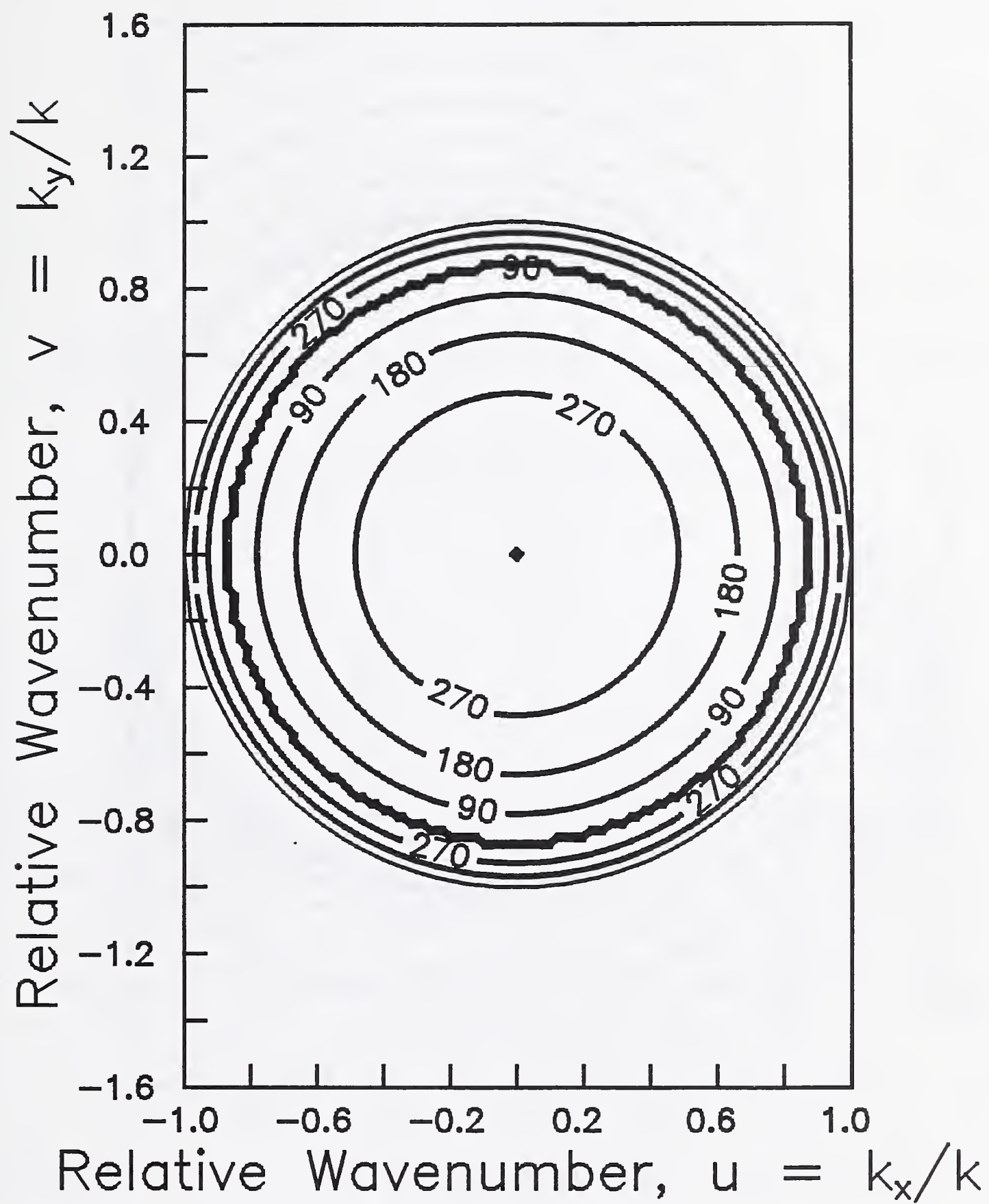
Figure 22. Phase of the factor exp(iγz). Frequency is 3 GHz and z = 20 cm.
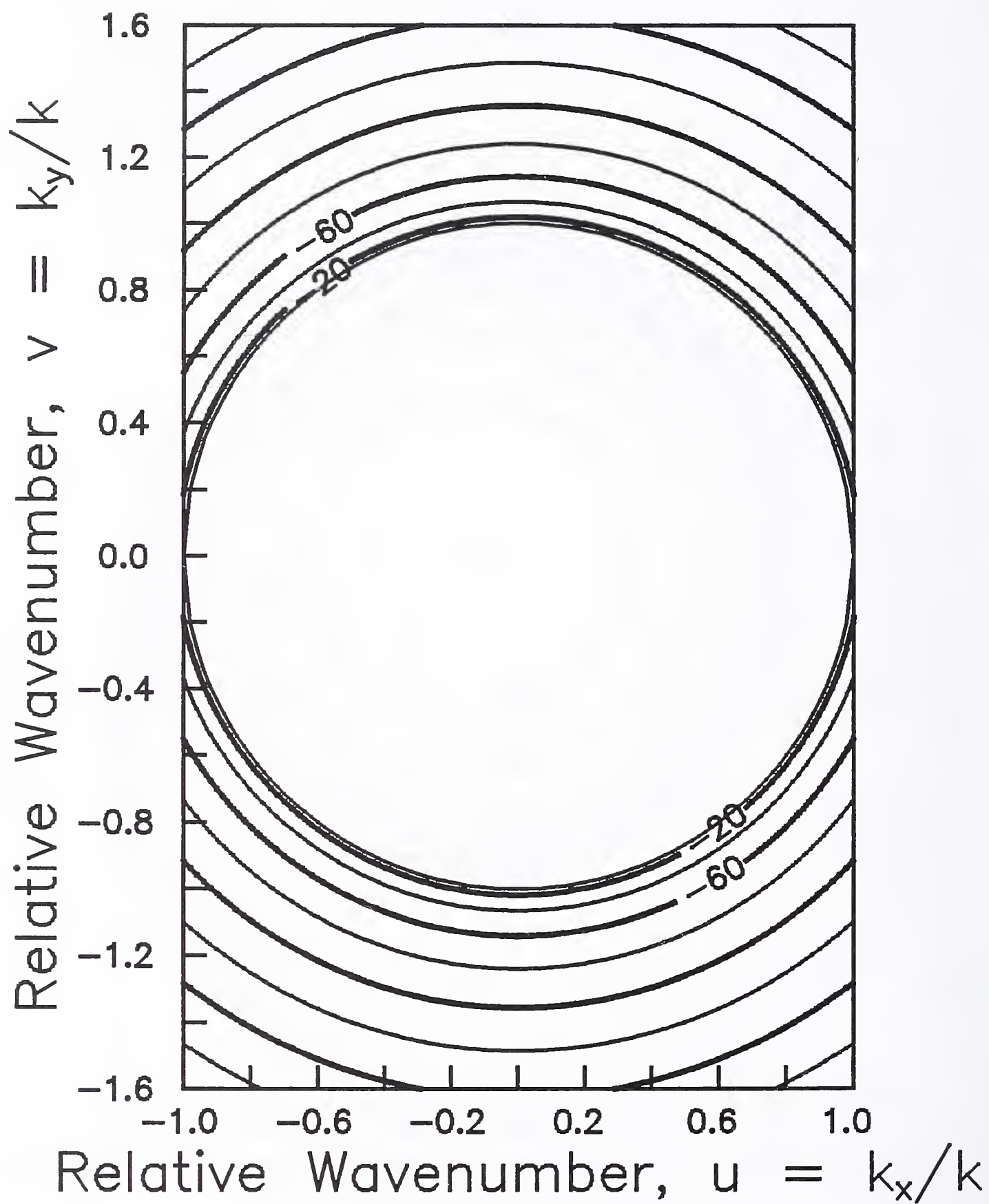
Figure 23. Amplitude of the factor exp(iγz). Frequency is 3 GHz and
z = 20 cm.
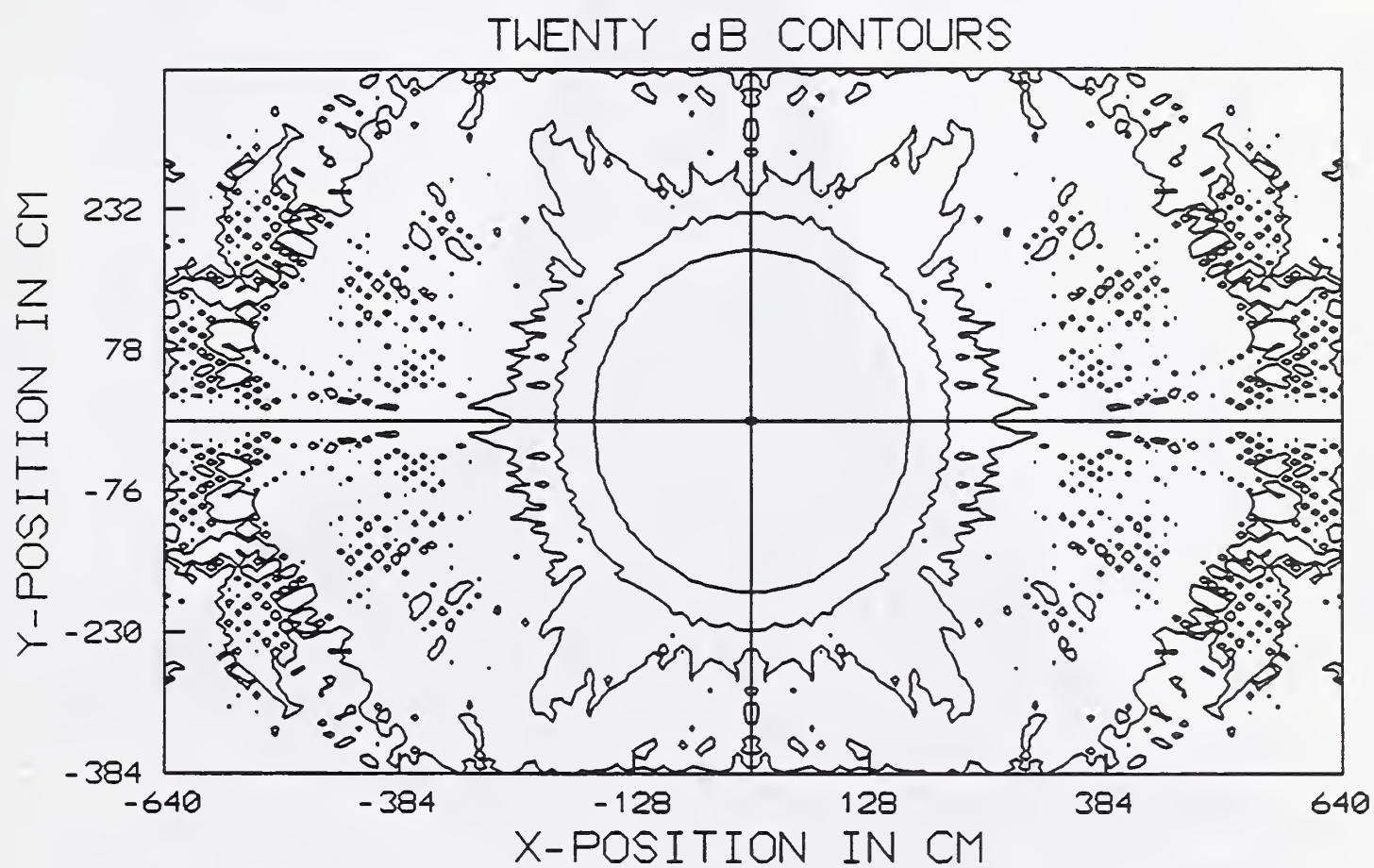
Figure 24. Simulated near-field amplitude. Frequency is 3 GHz and z = 20 cm.

NEAR-FIELD AMPLITDUE, Z=20 CM
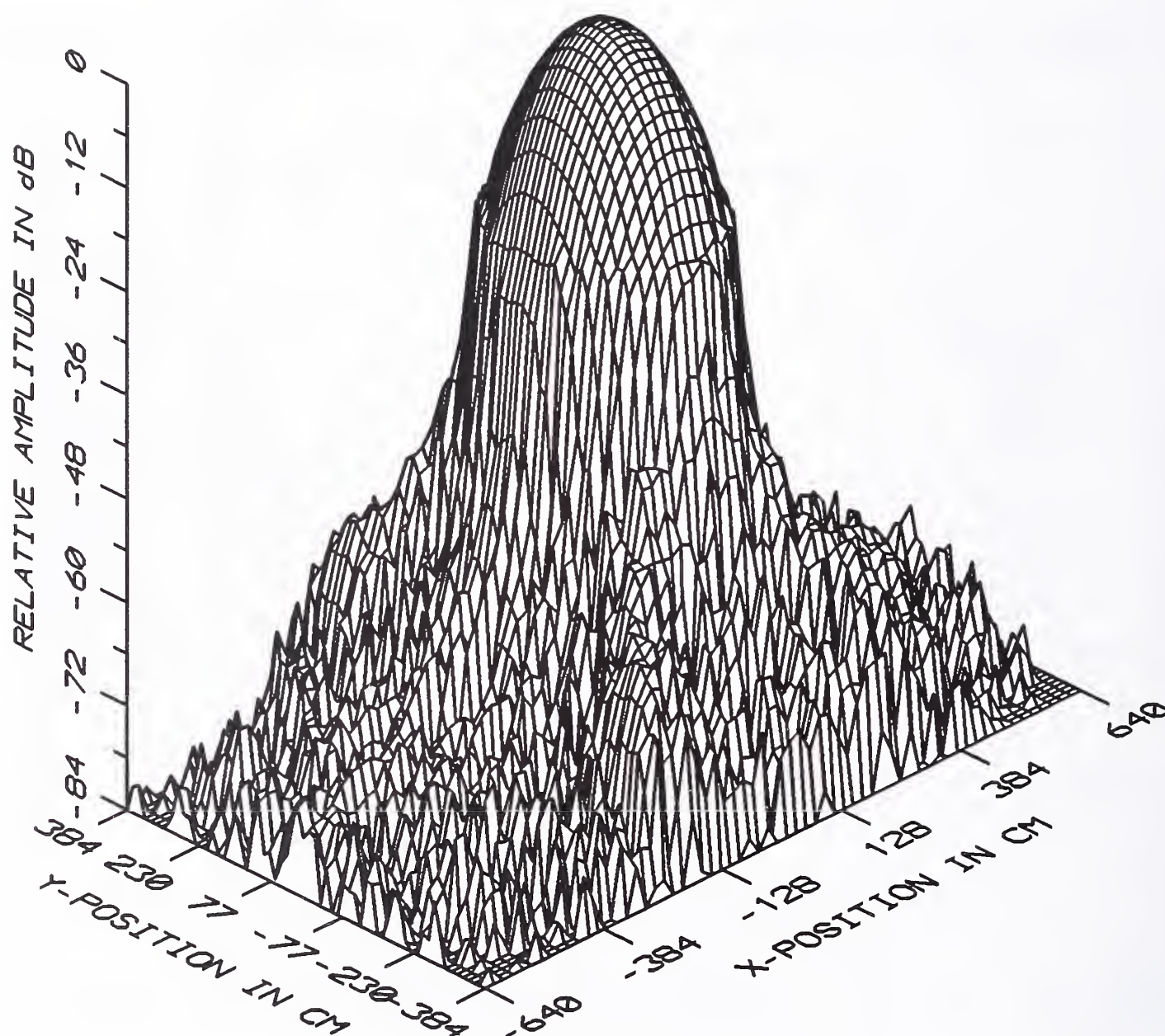
Figure 25. Perspective plot of the near-field amplitude. Frequency is 3 GHz
and z = 20 cm.
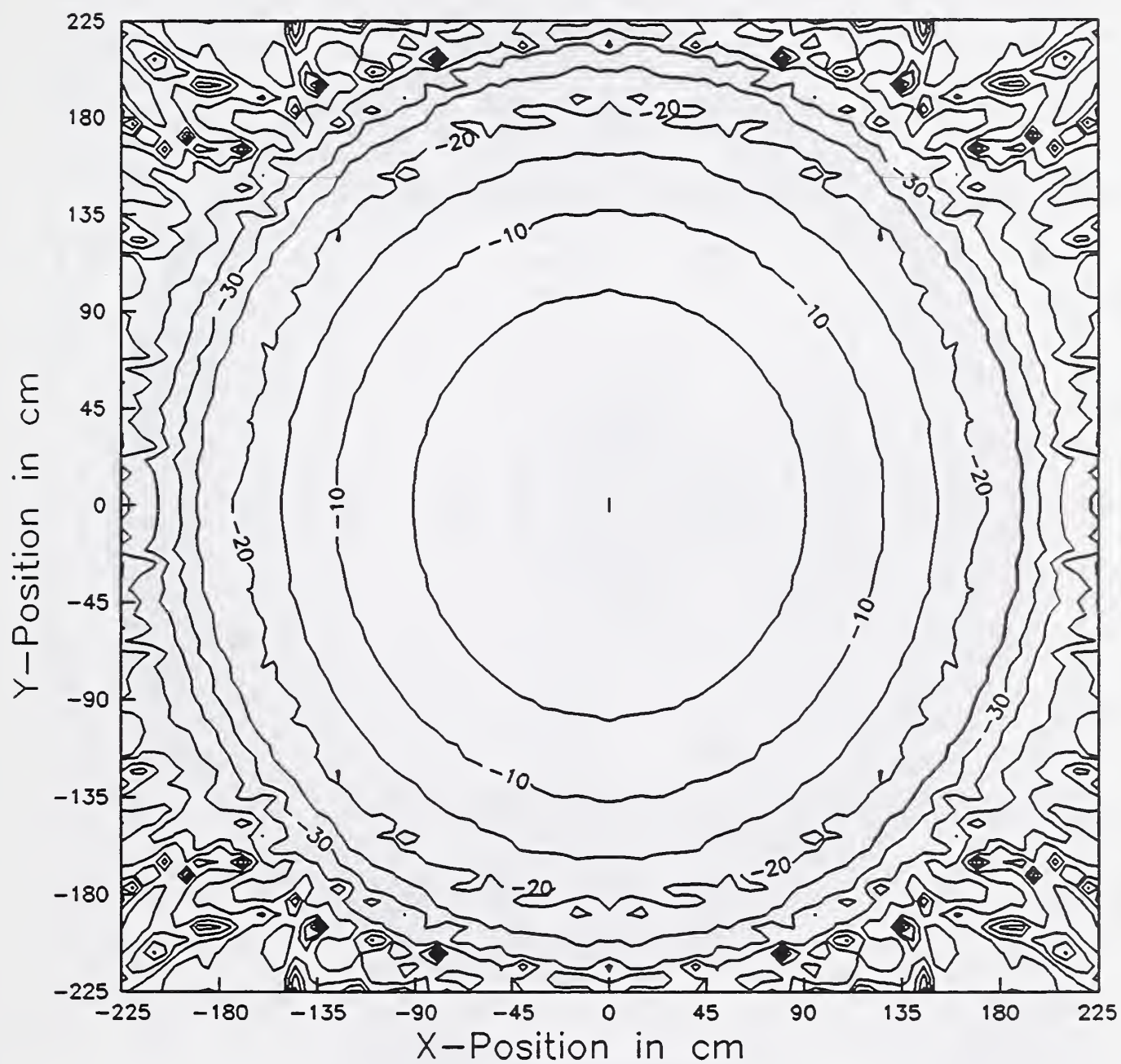
Figure 26. High resolution contour plot of the near-field amplitude near the center of the aperture. Frequency is 3 GHz and z = 50 cm.

Simulated Near–Field Phase z = 50 cm
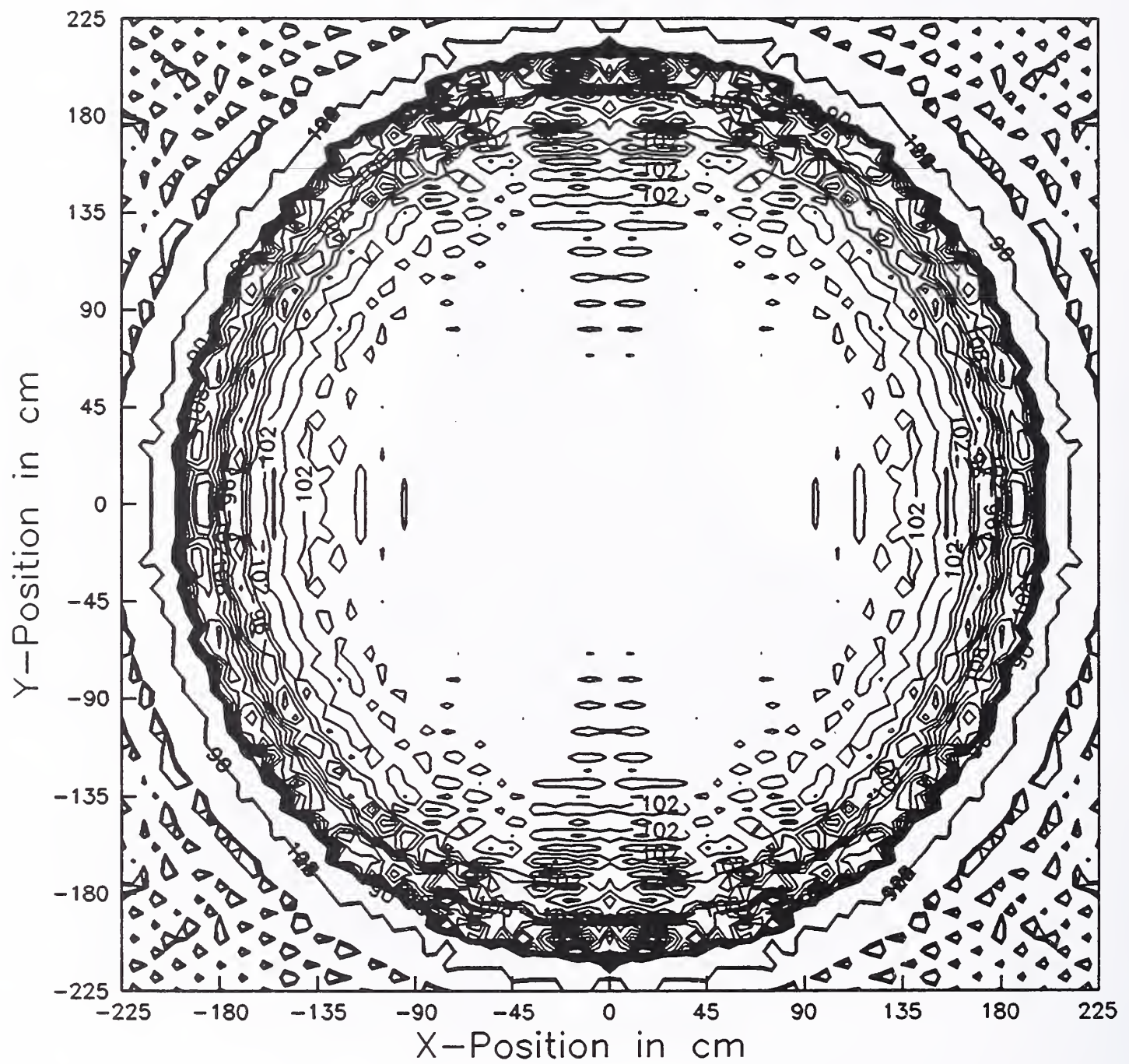
Figure 27. High resolution contour plot of the near-field phase near the center of the aperture. Frequency is 3 GHz and z = 50 cm.

10 dB Contours (0, −60)
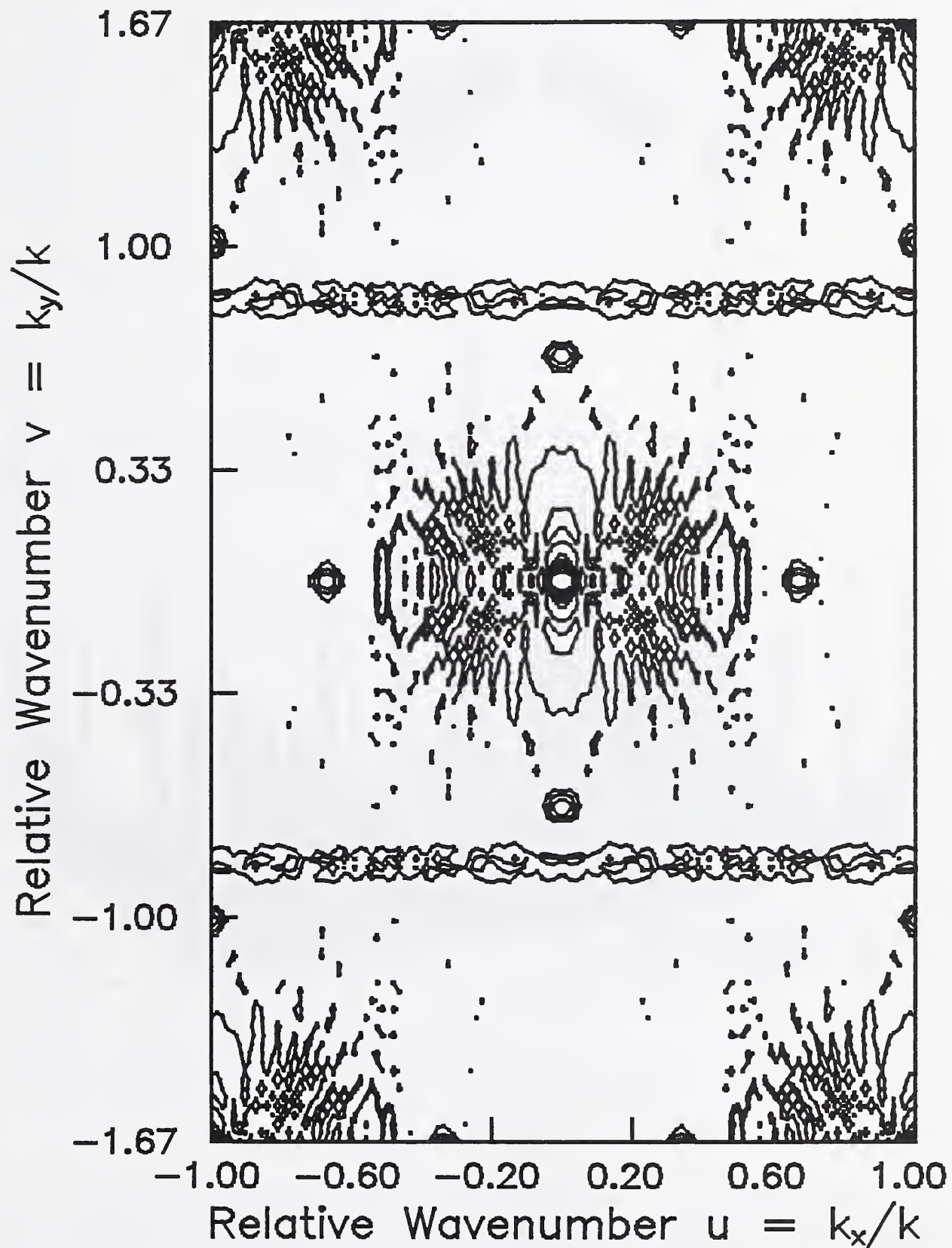
Figure 28. Contour plot of the array factor for an excitation matrix with sinusoidal phase errors in both x and y directions (3° amplitude, 15 cm period).
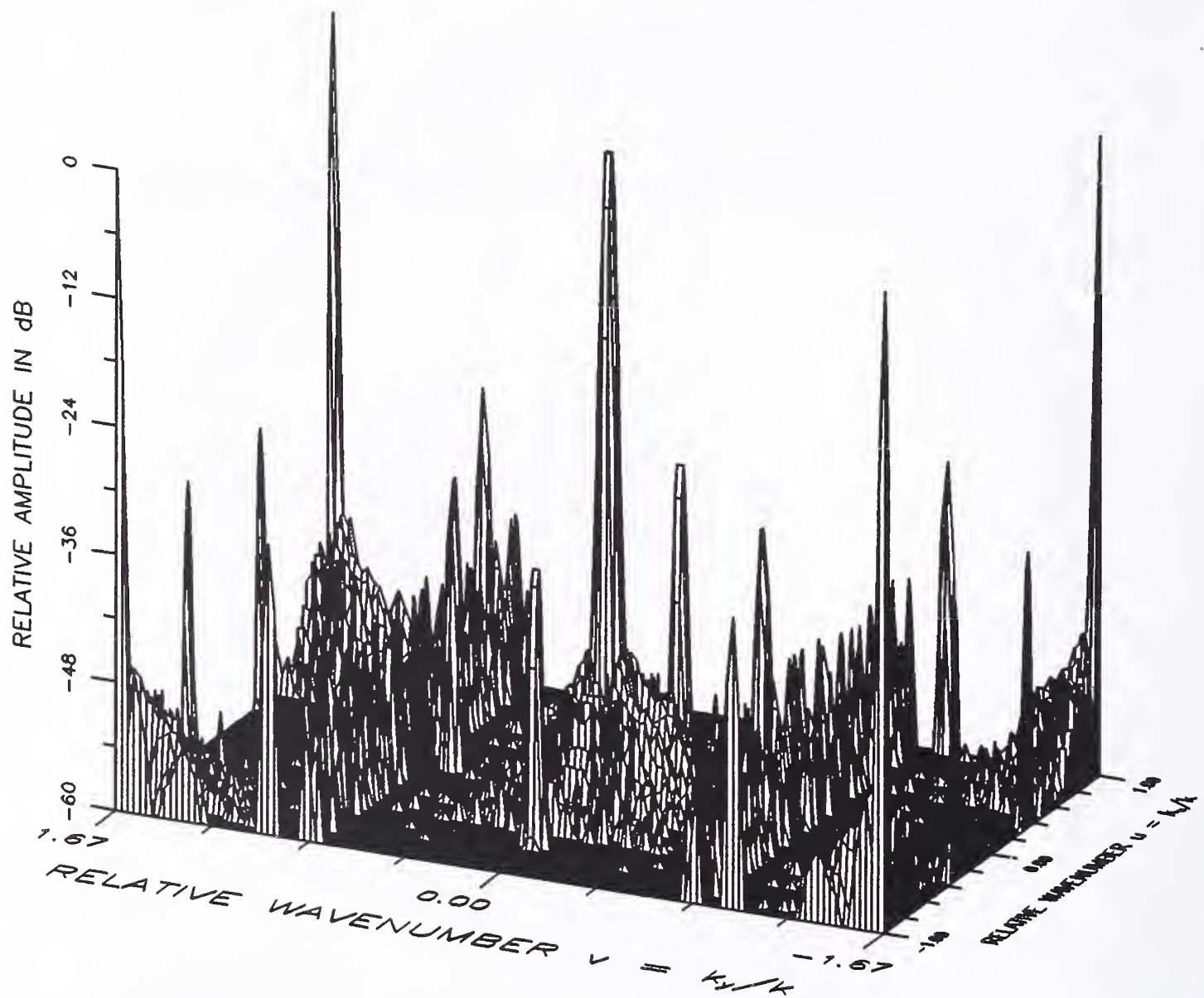
Figure 29.   Perspective plot of the array factor for an excitation matrix with
    sinusoidal phase errors in both x and y directions (3° amplitude, 15 cm
    period).
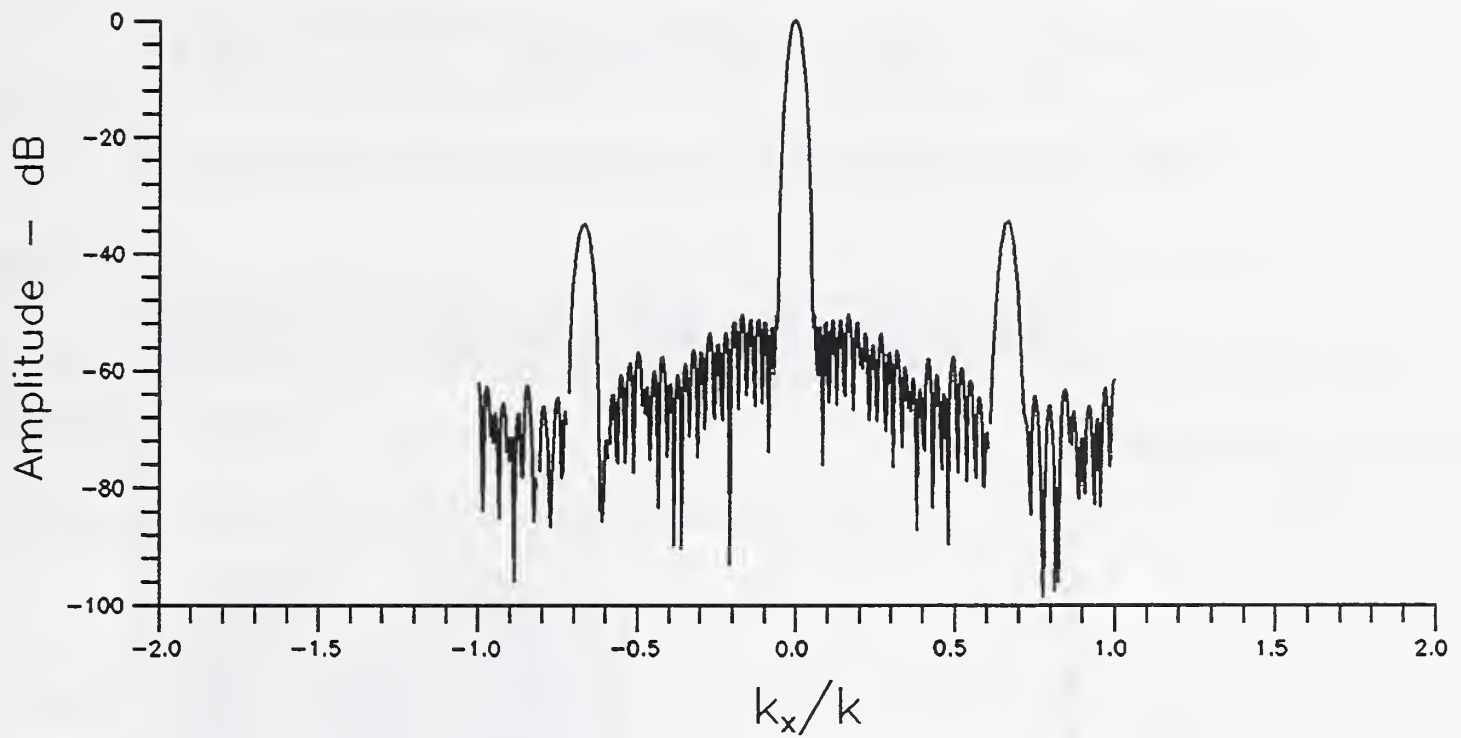
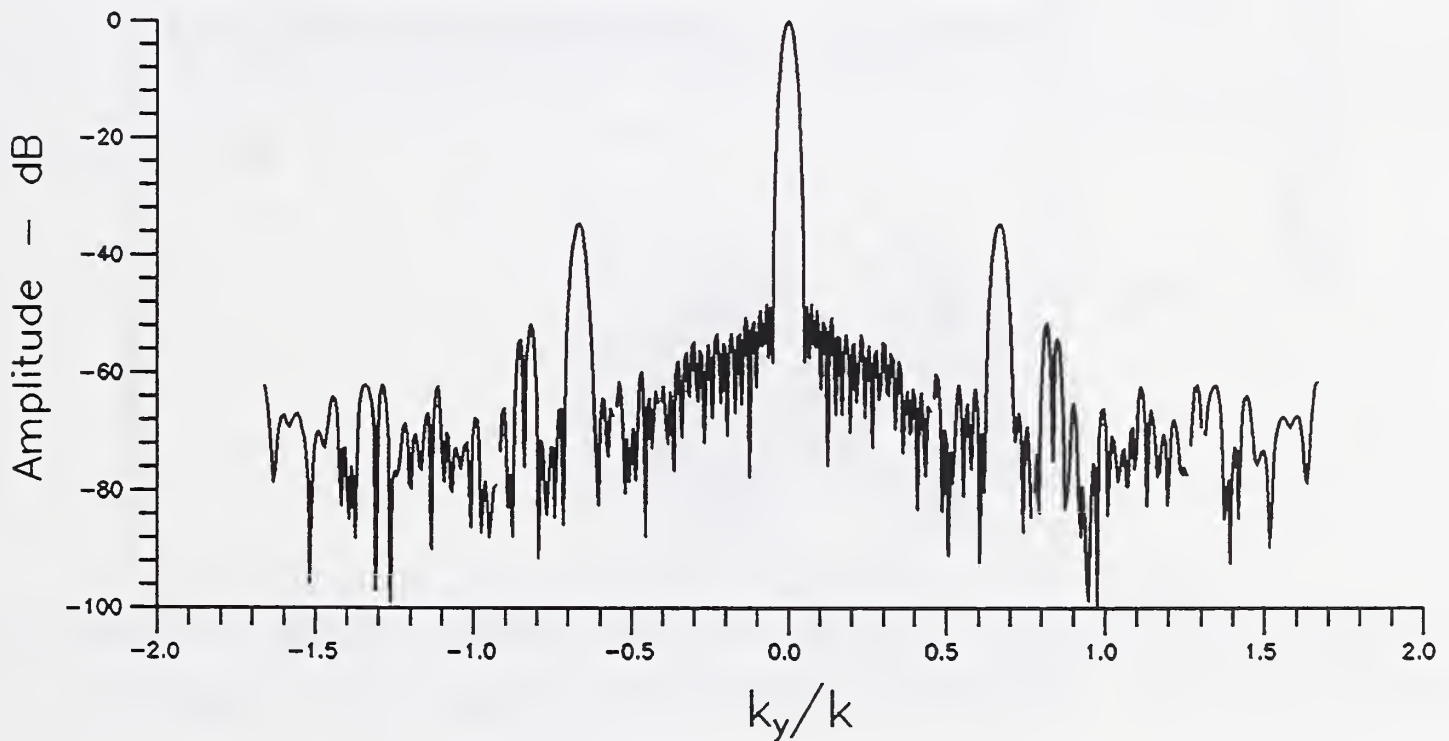Figure 30. Principal plane ($k_y = 0$) cut of the array factor for an excitation matrix with a sinusoidal phase error in the x direction (3° amplitude, 15 cm period).
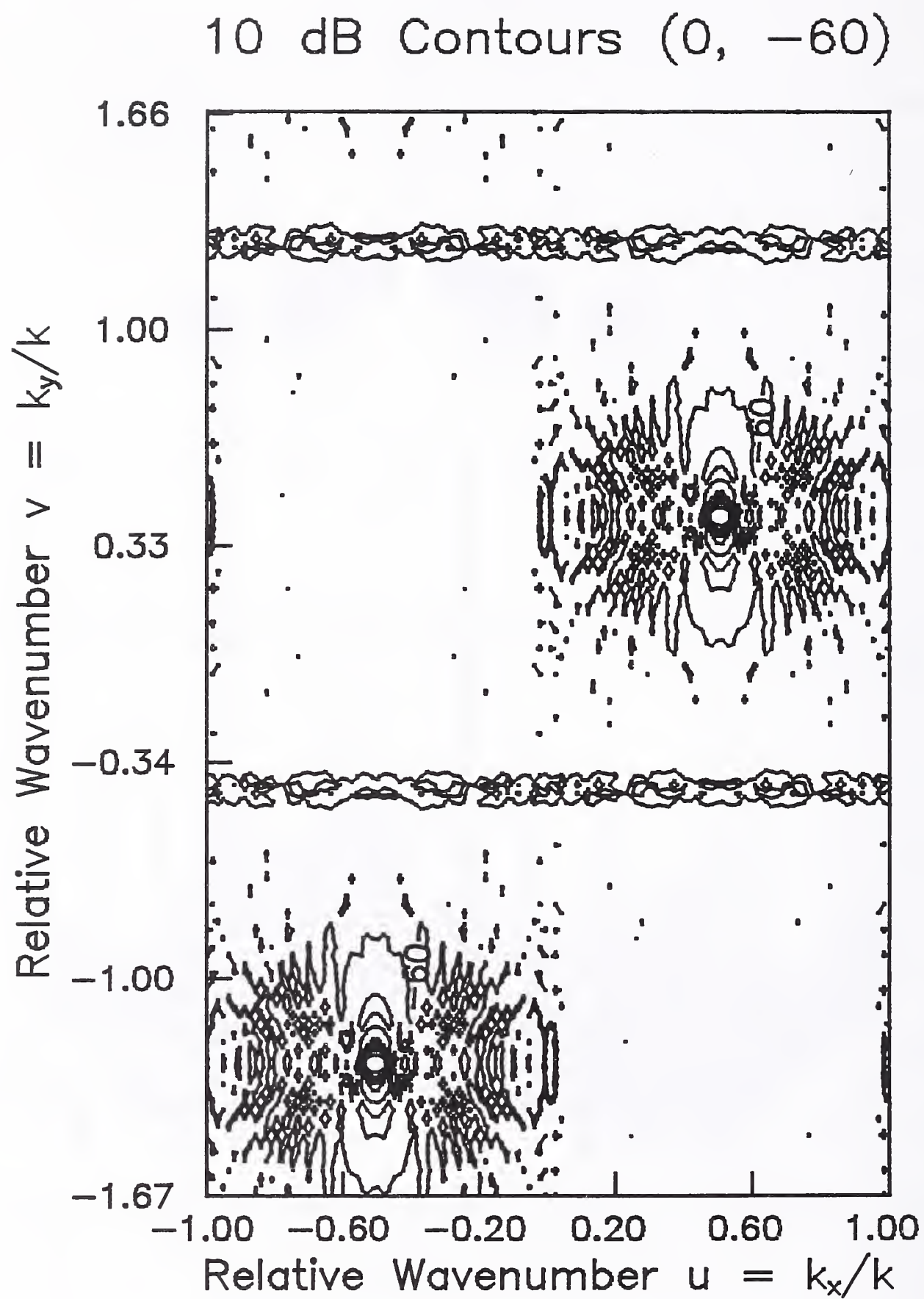

Figure 31. Principal plane ($k_x = 0$) cut of the array factor for an excitation matrix with a sinusoidal phase error in the y direction (3° amplitude, 15 cm period).

41

10 dB Contours (0, −60)

Figure 32.   Contour plot of array factor for a steered beam.

BL-114A (5-90) ADMAN 15.01	U.S. DEPARTMENT OF COMMERCE NATIONAL INSTITUTE OF STANDARDS AND TECHNOLOGY **BIBLIOGRAPHIC DATA SHEET**	1. PUBLICATION OR REPORT NUMBER NISTIR 3981
		2. PERFORMING ORGANIZATION REPORT NUMBER B92-0241
		3. PUBLICATION DATE OCTOBER 1992

4. TITLE AND SUBTITLE

Simulation of the Merged-Spectrum Technique for Aligning Planar Phased-Array Antennas, Part I

5. AUTHOR(S)

Ronald C. Wittmann, Allen C. Newell, Carl F. Stubenrauch, Katherine MacReynolds, Michael H. Francis

6. PERFORMING ORGANIZATION (IF JOINT OR OTHER THAN NIST, SEE INSTRUCTIONS) U.S. DEPARTMENT OF COMMERCE NATIONAL INSTITUTE OF STANDARDS AND TECHNOLOGY BOULDER, COLORADO 80303-3328	7. CONTRACT/GRANT NUMBER
	8. TYPE OF REPORT AND PERIOD COVERED

9. SPONSORING ORGANIZATION NAME AND COMPLETE ADDRESS (STREET, CITY, STATE, ZIP)

10. SUPPLEMENTARY NOTES

11. ABSTRACT (A 200-WORD OR LESS FACTUAL SUMMARY OF MOST SIGNIFICANT INFORMATION. IF DOCUMENT INCLUDES A SIGNIFICANT BIBLIOGRAPHY OR LITERATURE SURVEY, MENTION IT HERE.)

This report describes the initial phase of a NIST study of the merged-spectrum technique for determining the element excitations from planar scanning near-field measurements of phased-array antennas. Excitation data are used in adjusting phase shifters to meet design specifications. Measurement uncertainties, steering errors, and various analytic approximations will all introduce errors into the alignment. The study is ultimately directed to quantify the effect of these errors, to more fully understand the merged-spectrum technique and gives simulation examples illustrating calculation of near fields from array factor and element patterns.

12. KEY WORDS (6 TO 12 ENTRIES; ALPHABETICAL ORDER; CAPITALIZE ONLY PROPER NAMES; AND SEPARATE KEY WORDS BY SEMICOLONS)

antenna measurements; antenna array alignment; merged spectrum; near-field measurements; phased-array antennas; planar scanning.

13. AVAILABILITY	14. NUMBER OF PRINTED PAGES
[X] UNLIMITED	53
[ ] FOR OFFICIAL DISTRIBUTION. DO NOT RELEASE TO NATIONAL TECHNICAL INFORMATION SERVICE (NTIS).	
[ ] ORDER FROM SUPERINTENDENT OF DOCUMENTS, U.S. GOVERNMENT PRINTING OFFICE, WASHINGTON, DC 20402.	15. PRICE A04
[X] ORDER FROM NATIONAL TECHNICAL INFORMATION SERVICE (NTIS), SPRINGFIELD, VA 22161.	

ELECTRONIC FORM